2023 年度

ポリアミドメッシュ挿入による内部複雑構造を有する炭素繊維強化複合材料の損傷抑制に関する研究

Suppression of delamination in CFRP laminates with ply discontinuities using polyamide (PA) mesh material

補助事業報告書

2024 年 3 月

東京理科大学

創域理工学部機械航空宇宙工学科

助教 Fikry Mohammad

KEIRIN

競輪の補助事業　この報告書は、競輪の補助により作成しました。

http://jka-cycle.jp

Index

Chapter 1

Introduction

1.1 Carbon fiber reinforced plastics (CFRPs)

Carbon fiber reinforced plastics (CFRPs) are exceptionally strong and lightweight, making them ideal for use in various applications, including transport aircraft, automobiles, and more. Due to their superior strength-to-weight ratio compared to metals like aluminum and iron, and greater elasticity than titanium, CFRPs are particularly valued in the aerospace industry. Their adoption significantly cuts fuel consumption and CO_2 emissions throughout the lifecycle of products. For example, each Boeing 787 Dreamliner utilizes about 35 tons of CFRP, comprising roughly 50% of its structural components (Zhang et al., 2023).

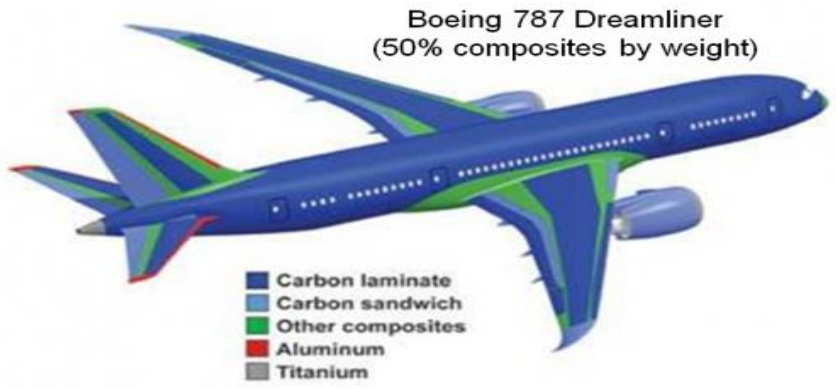

Fig. 1.1 Body structure of Boeing 787 (Forster et al., 2008).

The widespread adoption of CFRP across various industries has spurred extensive research into its damage, longevity, maintenance, and monitoring. Understanding the failure mechanisms of composite materials is essential for robust and cost-efficient engineering design. Major entities like National Aeronautics and Space Administration (NASA), Japan Aerospace Exploration Agency (JAXA), Boeing, and Airbus are heavily invested in multiscale experimental and analytical studies encompassing quantum mechanics, molecular dynamics, micromechanics, and structural analyses (NASA, accessed April 2024). This in-depth exploration of the complex failure processes in CFRP is crucial for enhancing its quality and performance in future applications.

All types of CFRP laminates are prone to accumulating microscopic damage such as matrix cracks and delamination, which limits their use to manufacturing structures within constrained strain levels (Fikry et al, 2017). Typically, cross-ply and angle-ply laminates experience transverse cracking in off-axis plies during tensile loading. These cracks often begin at the laminate's free edges and spread across the width. The formation of transverse cracking

impacts the mechanical properties of the laminates by reducing stiffness and causing residual strains, among other effects. Delamination, a form of secondary damage in CFRP laminates, often leads to laminate fracture. In addition to delamination, other secondary damage types include oblique and curved transverse cracks that form adjacent to straight cracks without any delamination. Specifically, oblique cracks in off-axis plies typically appear close to straight transverse cracks, while curved cracks tend to develop from two oblique cracks extending from the ply interface.

1.2 Ply/fiber discontinuity

Many researchers have explored the onset and growth of damage in various laminate configurations, but few have examined laminates with ply discontinuities, which are employed in industry to achieve cost-effective designs. By strategically cutting prepregs at certain locations, manufacturers can conserve material, leading to ply discontinuities. These discontinuities can compromise laminate strength due to stress concentrations. Moreover, in areas where fiber continuity is interrupted, resin pockets typically form during the curing process as the resin fills gaps left by absent or misaligned fibers. These resin-rich areas are normal in laminates, particularly in tapered structures like aircraft wings and rotor blades, which vary in thickness to optimize performance (Woigk et al., 2021). However, they introduce challenges such as stress concentration and potential delamination, with the resin pockets being inherently weaker and more prone to cracking (Fikry et al, 2023). It's crucial to assess how these discontinuities and the resultant resin pockets affect the mechanical properties and damage behavior of laminates. Fig. 1.2 illustrates the laminate with ply discontinuity (resin pocket).

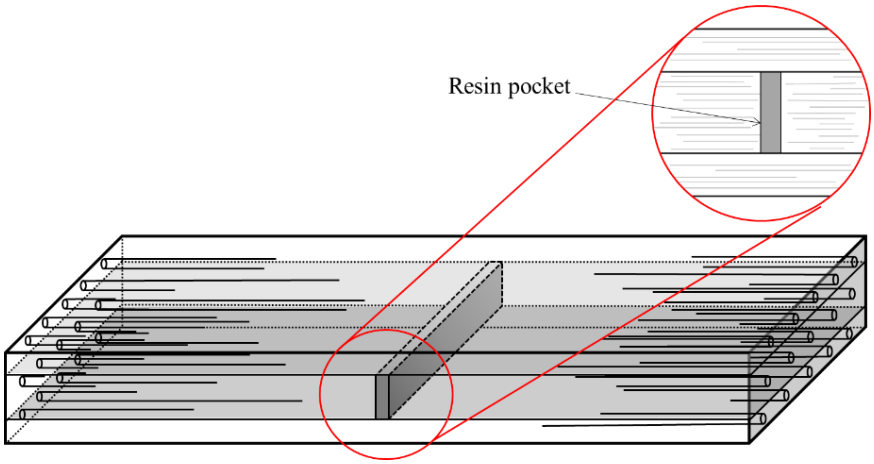

Fig. 1.2 Illustration of a laminate with ply discontinuity (resin pocket).

1.3 Interlaminar fracture toughness of CFRP laminates

Interlaminar fracture toughness is a crucial property of composite laminates, pivotal for their structural integrity and durability. This metric evaluates the laminate's capacity to resist crack propagation between layers—a critical issue as such phenomena can significantly undermine the mechanical performance of composite structures. Understanding and enhancing interlaminar fracture toughness is essential, particularly because it directly influences the prevention of

delamination, a prevalent failure mode in layered composites subjected to diverse loading conditions (Liu et al., 2020).

Interlaminar fractures in CFRP laminates are generally categorized into three primary modes. mode I, or the opening mode, involves the opening of a crack perpendicular to the laminate plane, typically induced by normal tensile stresses acting parallel to the crack front. This mode stresses the resin-rich interlayers, testing the laminate's resistance to peeling stresses. Mode II, or the Sliding Mode, occurs when layers slide over each other due to in-plane shearing forces parallel to the plane of the laminate but perpendicular to the crack front (Richard et al., 2016). Mixed-mode delamination involves a combination of these two stresses and is common in real-world applications where loading conditions are rarely uniform (Ou, et al., 2024). Understanding these modes is crucial for predicting failures accurately and designing materials that can withstand complex stress states.

The assessment of interlaminar fracture toughness is typically conducted using standardized test methods such as the Double Cantilever Beam (DCB) test for mode I, the End Notched Flexure (ENF) test for mode II, and various mixed-mode bending (MMB) tests for mixed-mode delamination. These tests help in precisely measuring the energy required to propagate a pre-introduced crack under controlled conditions, guiding modifications in composite design or manufacturing processes to improve fracture toughness (Simon and Banks-Sills, 2021).

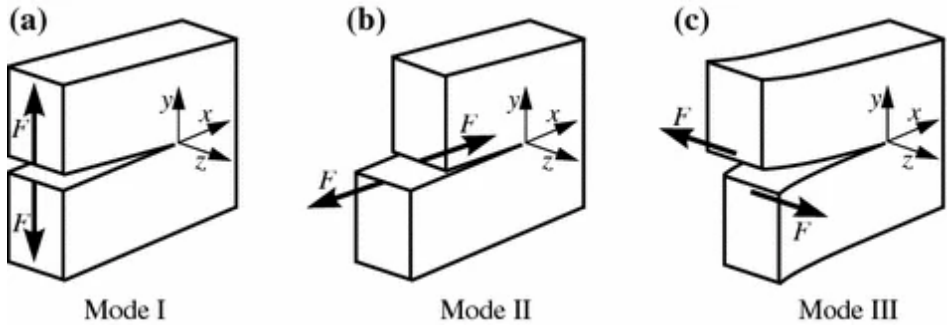

Fig. 1.3 Fracture modes (Richard et al., 2016).

1.4 Methods to improve the interlaminar fracture toughness of CFRP laminates

Improving interlaminar fracture toughness specifically addresses the prevention of delamination in CFRP laminates, which is crucial for maintaining the structural integrity of these composites under stress. Delamination is a prevalent failure mode where layers within the laminate separate, severely compromising the load-bearing capacity of the material (Huang and Bobyr, 2023). To combat this, several targeted strategies are employed.

Interleaf layers are particularly effective in enhancing interlaminar fracture toughness. By incorporating thin layers of toughened matrix materials or specialized films between the CFRP layers, these interleafs act as barriers that impede the initiation and propagation of delamination. They help to absorb impact and distribute stress across a broader area, thus reducing the concentration of stress at any single point that could lead to layer separation (Song et al., 2022).

Stitching and Z-pinning are direct mechanical reinforcement techniques aimed at increasing interlaminar toughness. By introducing high-strength threads or pins perpendicularly through the laminate layers, these reinforcements create physical bridges that connect the layers more robustly. This structural connection effectively limits the ability of the layers to separate under stress, significantly enhancing the resistance to delamination (Sun et al., 2005).

3D reinforcement architectures, such as 3D woven, knitted, or braided composites, also play a pivotal role in improving interlaminar toughness. These structures integrate reinforcement fibers in multiple dimensions, which inherently enhances the delamination resistance. The interconnected nature of the fibers throughout the thickness of the laminate helps to distribute loads more evenly and resist separation under mechanical or thermal stresses (Tong et al., 2002).

Additionally, the choice of resin plays a significant role in interlaminar fracture toughness. Toughened matrix systems, which can absorb more energy before failing, are particularly beneficial. These systems may include modified epoxies with added rubber or thermoplastic particles, which enhance the ability of the matrix to bridge and stop cracks that could otherwise lead to delamination (Zhao et al. 2020)

1.5 Polyamide (PA) mesh

Polyamide (PA) mesh (Fig. 1.4), commonly known as nylon mesh, is made from high-quality monofilament threads woven to create a precise mesh with exact apertures. The size of these apertures, determined by the number of threads per unit area and the thickness of these threads, defines the mesh's filtration capacity. This mesh exhibits excellent wear resistance and high resistance to various chemicals, making it a durable choice in harsh environments. It withstands high temperatures, with a melting point around 230°C, although it is sensitive to acids and UV light (Topzeven Homepage, accessed April 2024).

One prominent use of PA mesh is in filtration, where it excels in environmental and industrial settings, filtering everything from water to air and various chemicals. Its precision in aperture sizes makes it highly effective for these purposes. Additionally, PA mesh is integral to the screen-printing industry, favored for its durability and compatibility with various inks and dyes, essential for producing high-quality prints. In the medical field, PA mesh is utilized in devices such as surgical meshes for hernia repairs, benefiting from its biocompatibility and robust physical properties. The automotive industry also employs PA mesh in air filtration systems, enhancing engine performance and cabin air quality. Beyond these applications, PA mesh finds a place in textiles, particularly in sports and athletic wear, due to its resistance to abrasion and mildew, as well as in luggage linings. Furthermore, PA mesh serves significant roles in agriculture and horticulture, commonly used as protective netting against pests and as part of aquaculture systems for containing fish or growing marine plants. This wide array of applications highlights PA mesh's versatility and the broad reliance on its unique material properties across industries Jason Mills LLC, <Accessed April 2024>.

Fig. 1.4 Polyamide (PA) mesh (Bonfilt <Accessed April 2024>).

1.6 Objectives

The widespread application of CFRP in structural components is limited by their inferior out-of-plane properties, such as interlaminar toughness, despite their excellent in-plane characteristics. This deficiency becomes particularly problematic in complex structural components of CFRPs, such as tapered sections for thickness variation, bolt holes for joints, and areas involving adhesives and joints. These are typically the initial sites of intra-laminar damage, which subsequently act as triggers for interlaminar failures. The absence of established optimal design methods for real structures that incorporate these complexities presents a significant challenge. This study aims to address this gap by utilizing PA mesh as an innovative solution to enhance the interlaminar fracture toughness and suppress the onset of interlaminar damage in CFRP laminates. By investigating its effective placement within the laminate structure, this research seeks to develop a method that not only optimizes the structural design of complex CFRP laminates but also contributes to lightweight construction in transport equipment.

Chapter 2

Fracture toughness evaluation

2.1 Mode I fracture toughness evaluation (Double cantilever beam (DCB) test)

To obtain the mode I interlaminar fracture toughness values, a Double Cantilever Beam (DCB) test was conducted. Details regarding the dimensions of the test specimens, the testing procedure, and the method for calculating the Mode I interlaminar fracture toughness values are documented below.

2.1.1 Materials and specimen manufacturing

For the manufacture of test specimens for interlaminar fracture toughness evaluation, prepreg (T700SC/2592, manufactured by Toray Industries) with a thickness of 0.14 mm was used. The carbon fiber T700SC is made from polyacrylonitrile, and the resin consists of epoxy resin 2592. Additionally, the carbon fiber has a weight content of 67%, and the epoxy resin has a weight content of 33%. As the specimens for the interlaminar fracture toughness test, a unidirectional (UD) $[0]_{20}$ laminate was manufactured. The prepregs, each with a thickness of 0.14 mm per ply, were cut into 20 pieces of 200 x 200 mm. These were then stacked up into two sets of 10 pieces each. As shown in Fig. 2.1, a PA mesh, measuring 175 x 200 mm was sandwiched between these two sets of stacked prepregs. The PA mesh used in this study has a fiber diameter of 50 µm, a thickness of 87 µm, and an opening of 95 µm (N-NO175T, NBC Meshtec Inc.). To create an initial crack in the specimen, polyimide film, measuring 25 x 200 mm was also sandwiched in between the upper and lower plies. The polyimide film used was 25 µm thick. An autoclave (DANDELION 2010) was used to cure the laminate at 130°C and a pressure of 0.2 MPa. Laminates are cut into the measurement shown in Fig 2.2 and Table 2.1 by using a composite material cutting machine (AC-300CF, Maruto Testing Machine).

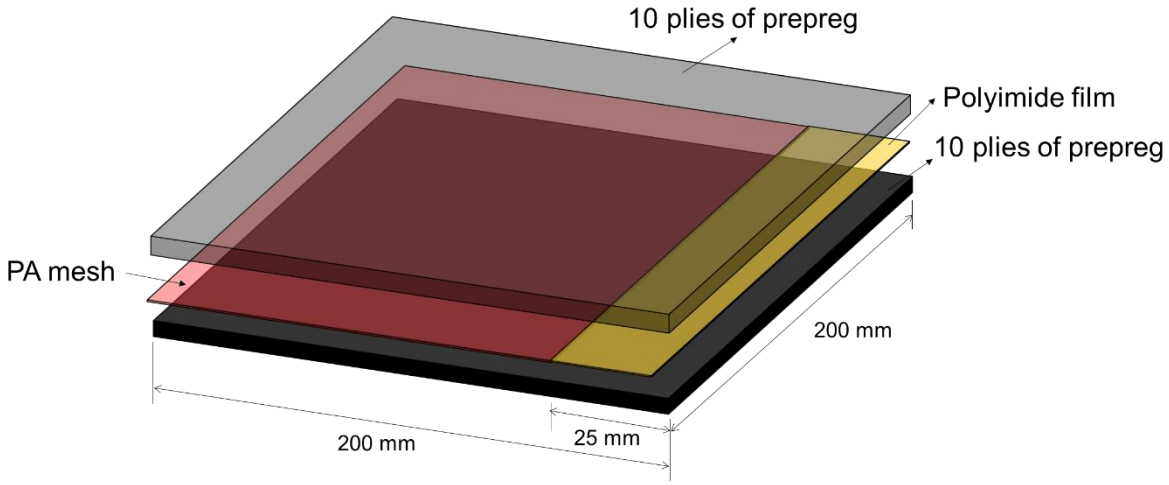

Fig. 2.1 Illustration of the lay-up structure of a laminate for interlaminar fracture toughness evaluation.

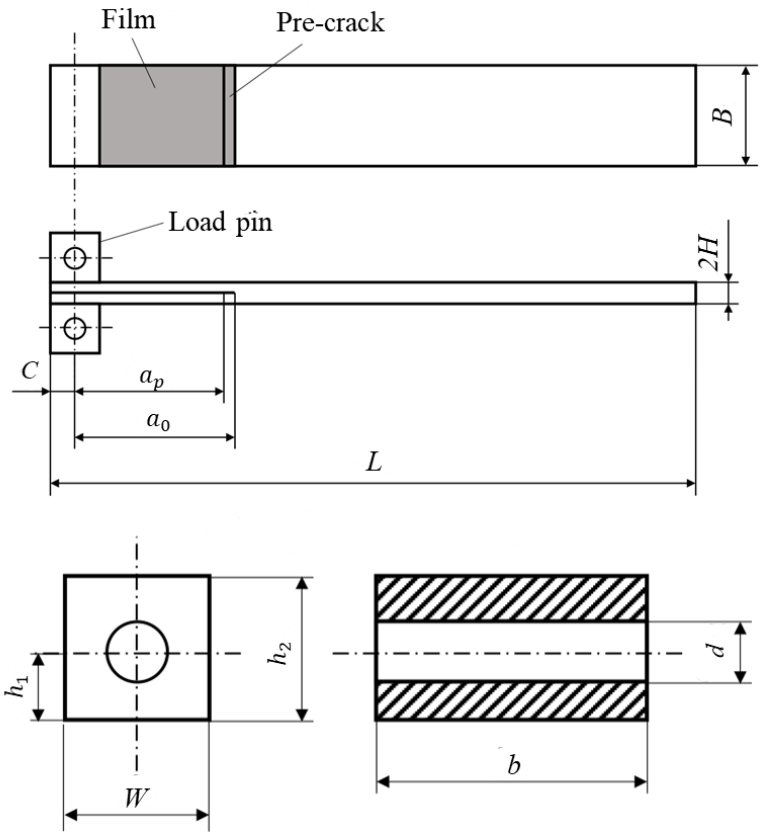

Fig. 2.2 Schematic specimen configuration for DCB test.

Table 2.1 Specimen dimension for DCB test.

	Symbol	Parts	Size [mm]
DCB specimen	L	Length	90
	$2H$	Thickness	2.3
	B	Width	10
	C	Distance from specimen end load line	6
	a_p	Film crack length	25
	a_0	Pre-crack length	28-32
Load pin	W	Width	12
	b	Length	12
	h_1	Half height	6
	h_2	Height	12
	d	Hole diameter	5

The edges of the specimens manufactured were polished using a polisher (Tegrapol 15, Struers), with water as the lubricant and waterproof abrasive paper (Marumoto Manufacturing) for grinding. The polishing was conducted for 1 minute with a grit size of 500, 1 minute 30 seconds with a grit size of 1000, 2 minutes with a grit size of 2000, and 2 minutes 30 seconds with a grit size of 4000. Subsequently, a diamond spray (DP Spray, Struers) was used to adhere diamonds to the surface, performing diamond polishing for 3 minutes. Afterward, the polished edges were examined using a digital microscope (VHX-2000, Keyence).

2.1.2 DCB test method

DCB tests were carried out using a universal testing machine (SC-5H, JT Torsi Co.). In this study, measurements were taken of the load P, crack length a, and crack opening displacement (COD). Five specimens were tested. The first measurement was taken when the crack had propagated 3 mm from the initial crack, and subsequent measurements were made every 3 mm of crack propagation, with a total of five measurements per specimen. The loading speed was set at 0.5 mm/min up to 6 mm from the initial crack, and increased to 1.0 mm/min for crack propagation beyond 6 mm. Unloading was performed at a rate of 5.0 mm/min after each measurement. A measuring microscope (VHX-1000, Keyence) was used to measure the crack length. Mode I interlaminar fracture toughness value G_I, was calculated using the following formula:

$$G_I = \frac{3}{2(2H)}\left(\frac{P_C}{B}\right)^2 \frac{(B\lambda)^{\frac{2}{3}}}{\alpha_1} \tag{2.1}$$

G_I was determined using the critical load P_C, the compliance of the COD in the elastic portion of the load-COD curve λ, and the slope of the linear approximation of the cube root of the compliance of the normalized crack length per unit width α_1.

2.1.3 Results and discussion

Fig. 2.3 presents the results from the DCB tests. Figs. 2.3(a) to 2.3(e) display the results for each specimen, specifically specimens 1 through 5. In these figures, panel (i) illustrates the load–COD curves from the DCB test, panel (ii) depicts the normalized crack length–compliance relationship (the equation in the figure represents the slope of the linear approximation α_1 and panel (iii) shows the mode II fracture toughness, G_I, as a function of crack length.

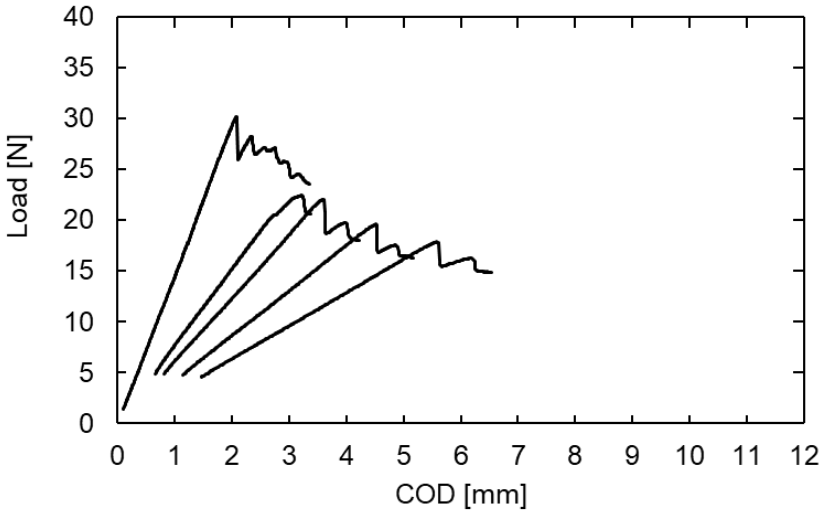

(i) Load–crack opening displacement (COD) curves from DCB test.

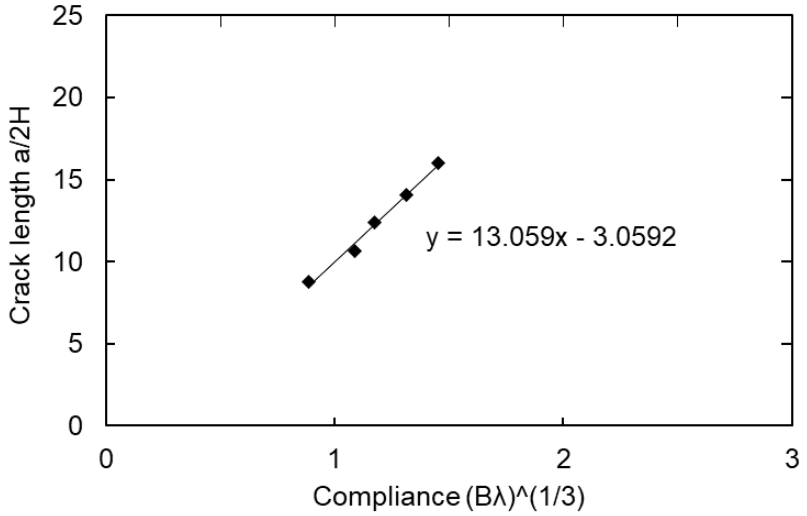

(ii) Normalized crack length–compliance relationship.

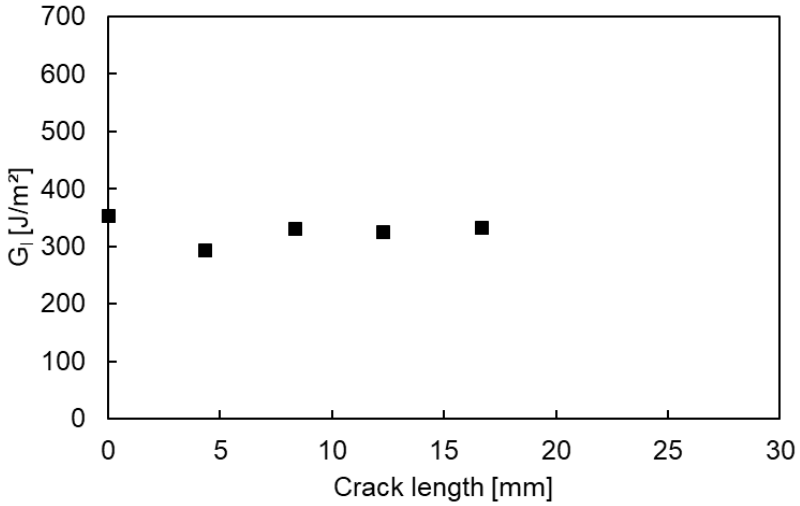

(iii) Mode II fracture toughness G_I–crack length relationship.

(a) Specimen 1

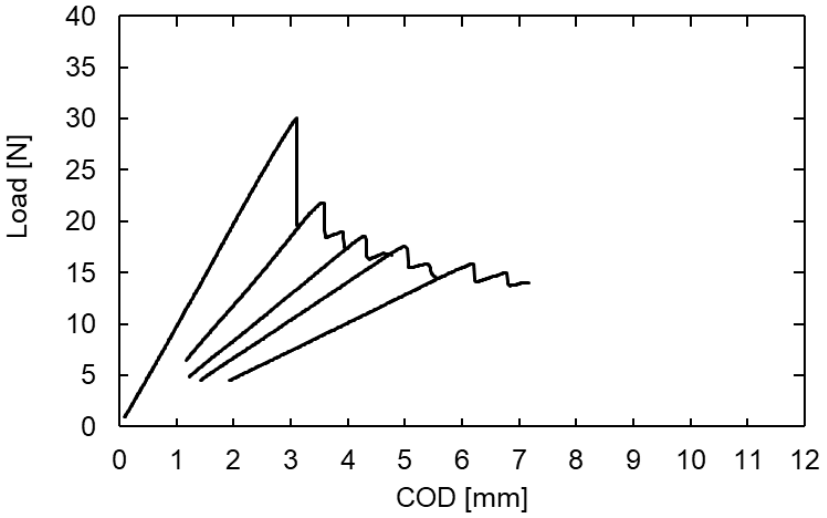

(i) Load–crack opening displacement (COD) curves from DCB test.

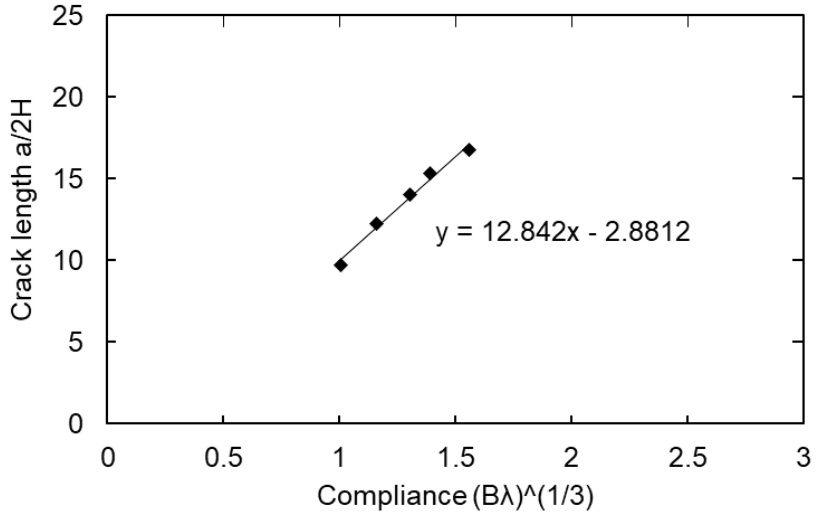

(ii) Normalized crack length–compliance relationship.

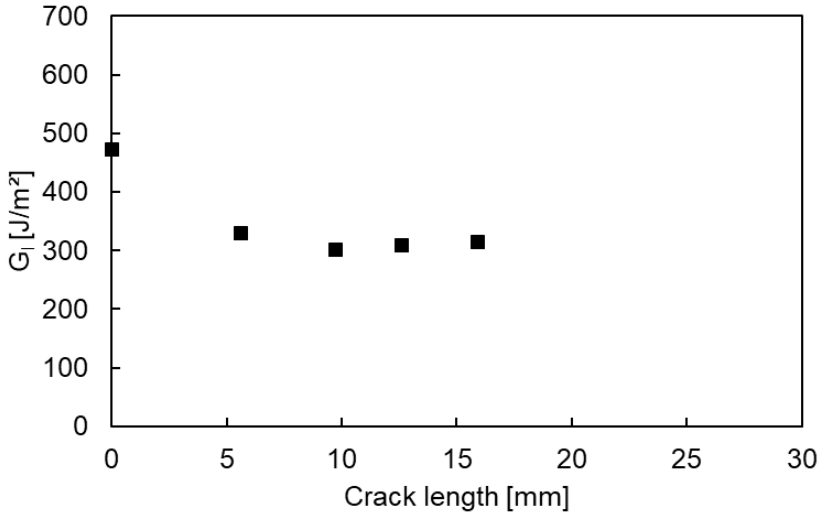

(iii) Mode II fracture toughness G_I–crack length relationship.

(b) Specimen 2

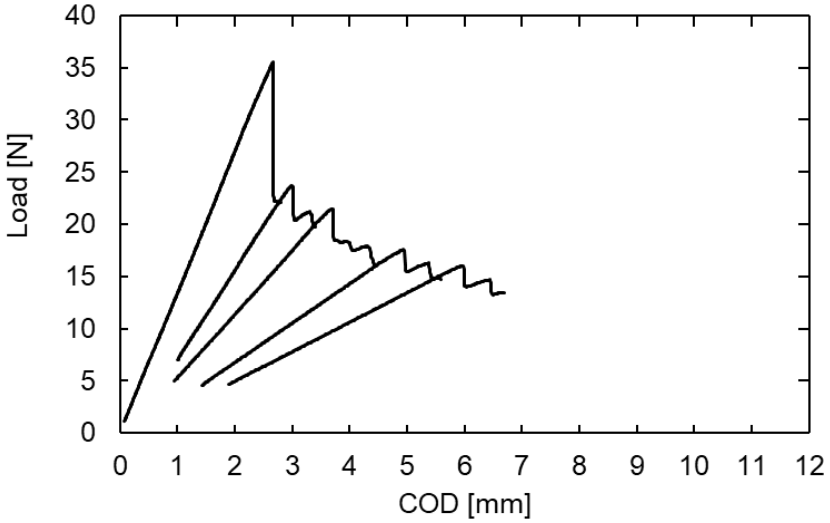

(i) Load – crack opening displacement (COD) curves from DCB test.

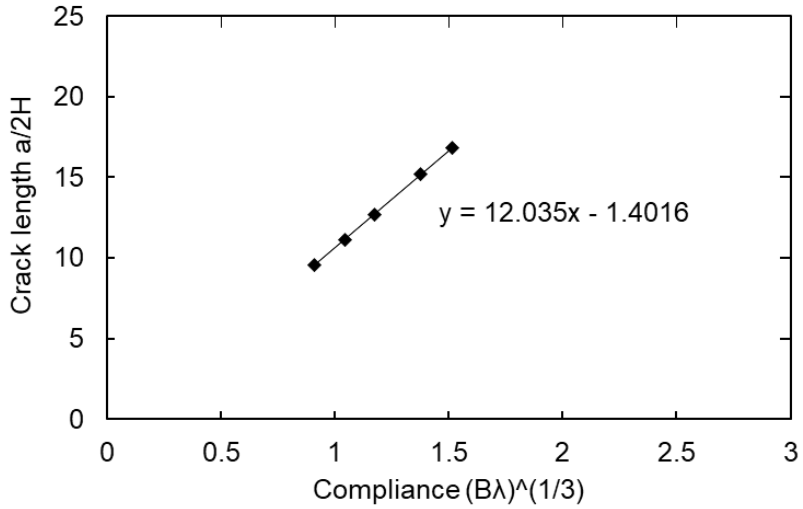

(ii) Normalized crack length – compliance relationship.

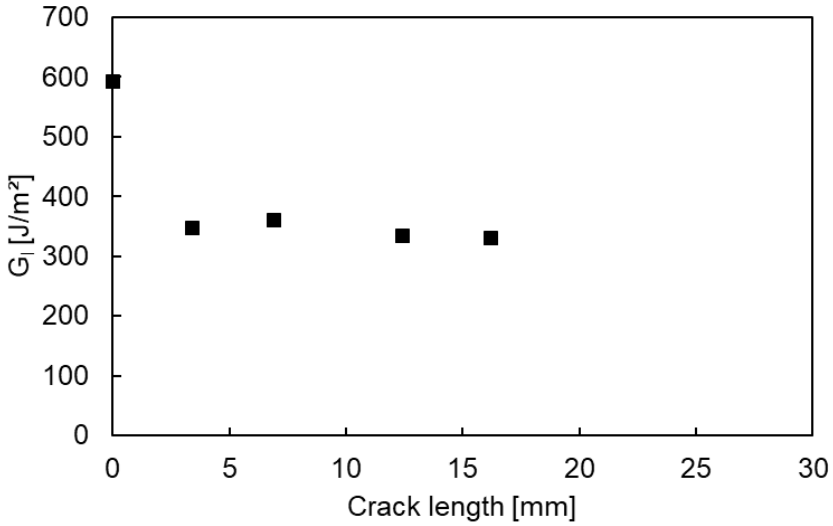

(iii) Mode II fracture toughness G_I – crack length relationship.

(c) Specimen 3

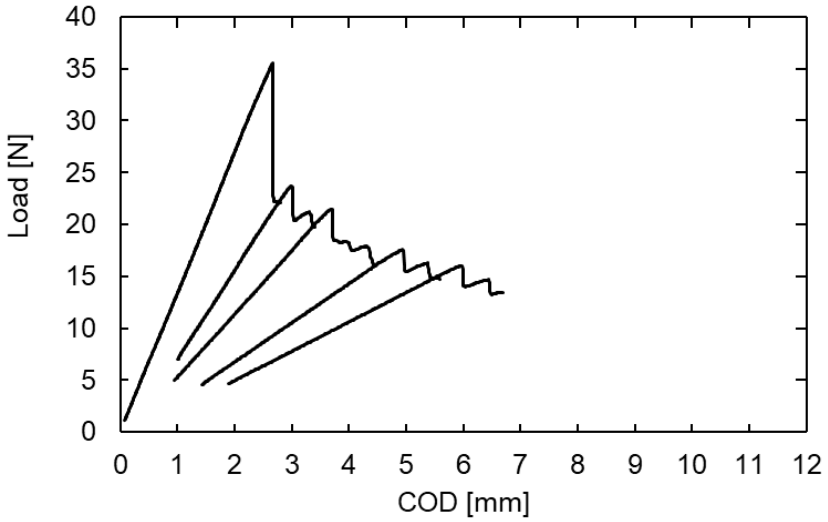

(i) Load – crack opening displacement (COD) curves from DCB test.

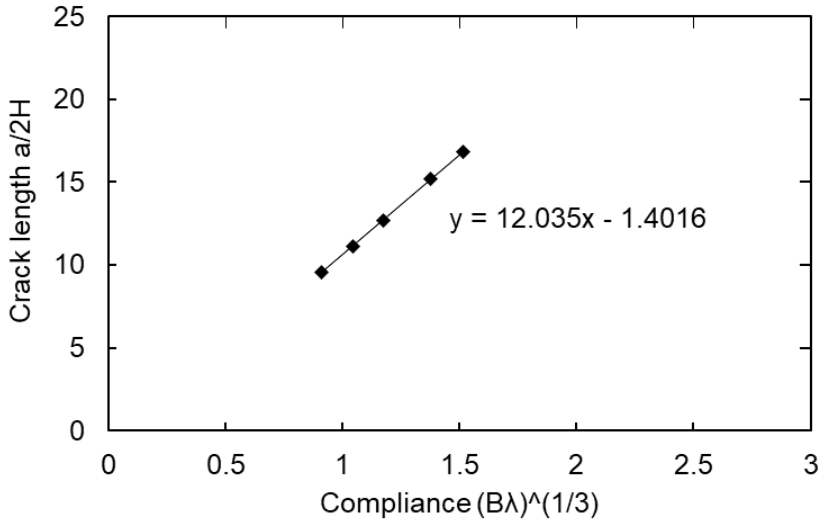

(ii) Normalized crack length – compliance relationship.

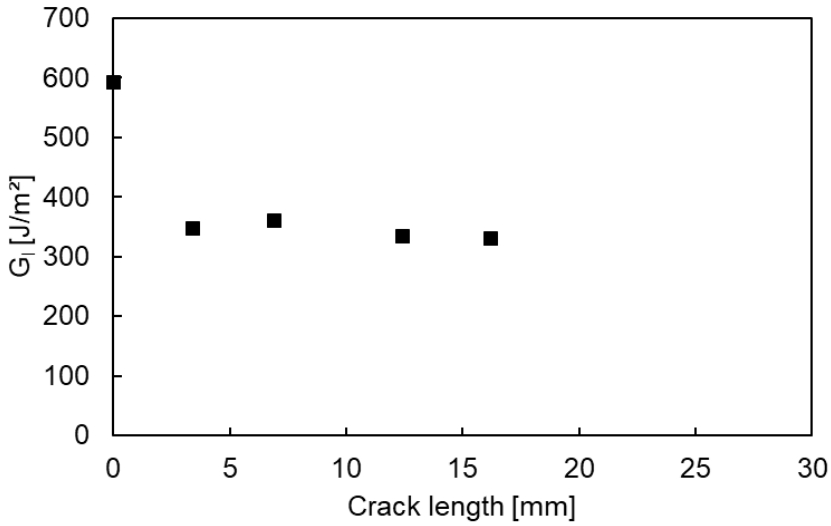

(iii) Mode II fracture toughness G_I – crack length relationship.

(d) Specimen 4

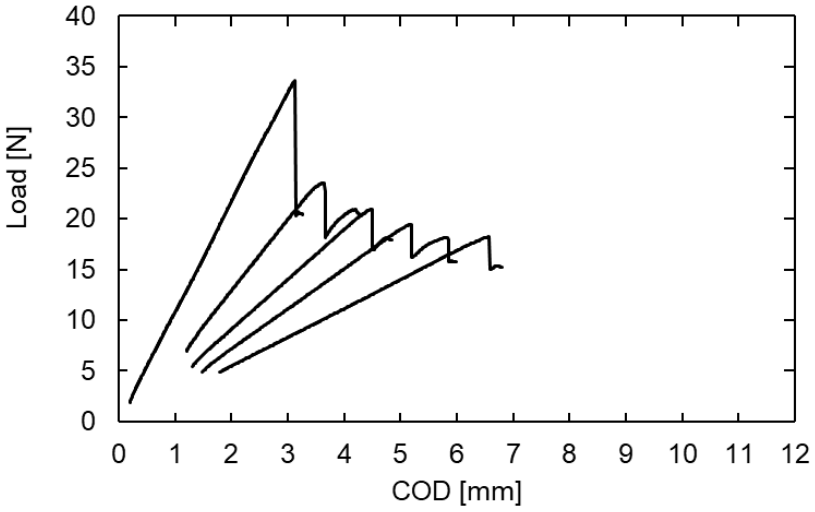

(i) Load – crack opening displacement (COD) curves from DCB test.

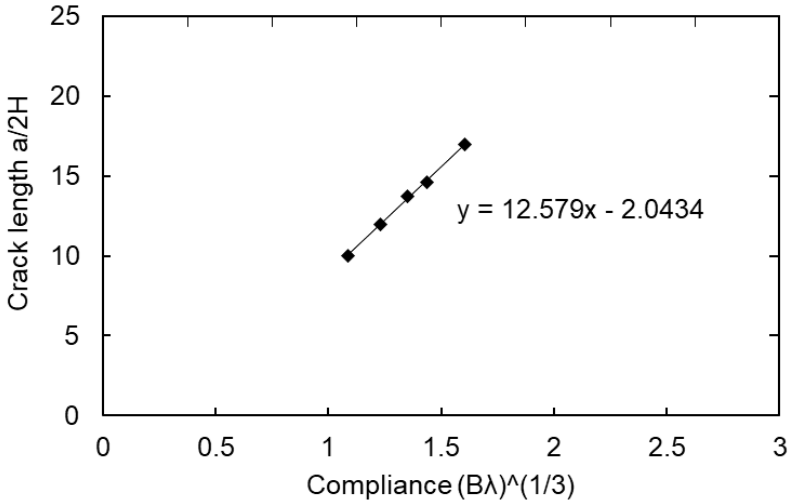

(ii) Normalized crack length – compliance relationship.

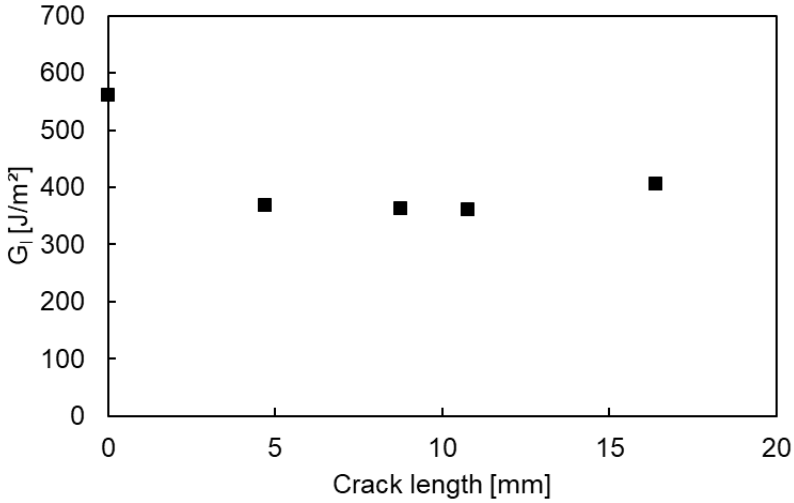

(iii) Mode II fracture toughness G_I – crack length relationship.

(e) Specimen 5

Fig. 2.3 Results from DCB tests of each specimen tested.

Fig. 2.4 shows the mode I fracture toughness G_I – crack length relationship for all specimens. Here, the dotted lines show the average G_I values. Table 2.2 summarizes the G_I values for all five specimens. G_{IC} is the fracture toughness value calculated from the first loading and represents the critical strain energy release rate necessary for the initiation of delamination. It quantifies the energy per unit area required to initiate a delamination under mode I loading conditions. Conversely, G_{IR} represents the average fracture toughness value from the second to the fifth loading. This parameter is the propagation strain energy release rate, which measures the energy required to propagate an existing delamination. The average G_{IC} and G_{IR} for all five specimens are 519 J/m² and 336 J/m², respectively.

Fig. 2.5 displays bar charts comparing the G_{IC} and G_{IR} values of neat CFRP laminate (specimen without PA mesh insert) and CFRP laminate with PA mesh insert. The G_{IC} value for the CFRP with PA mesh insert is approximately three times higher than that of the neat CFRP, which has a G_{IC} value of 171 J/m². However, it should be noted that the G_{IR} value is slightly reduced compared to the neat CFRP (366 J/m²). This indicates that inserting PA mesh into the CFRP laminate requires higher strain energy to initiate delamination, but once initiated, the propagation becomes easier under Mode I loading conditions. This indicates that the dimensions and configurations of the PA mesh used in this study are not optimal for enhancing the interlaminar fracture toughness performance of CFRP laminates under mode I loading.

To further investigate this, a structured study on the dimensions and configurations of PA mesh inserts should be conducted. Future studies should systematically vary the mesh size, strand thickness, and orientation to determine the optimal mesh design that maximizes fracture toughness without significantly compromising the composite's overall properties. This could involve a factorial design experiment where each variable is tested at multiple levels to assess their individual and interactive effects on the initiation and propagation of delamination under mode I loading conditions. The goal will be to identify an optimum set of measurements for the PA mesh that balances increased resistance to crack initiation with controlled crack propagation capabilities.

Table 2.2 Summary of the mode I fracture toughness G_I values of all five specimens of CFRP laminate with PA mesh insert.

Loading	Specimen					Average
	1	2	3	4	5	
1st	352	473	592	562	619	
2nd	292	329	347	370	345	
3rd	329	302	361	364	339	
4th	325	309	333	362	324	
5th	332	314	331	407	308	
G_{IC} [J/m²]	352	473	592	562	619	519
G_{IR} (ave.) [J/m²]	320	314	343	376	329	336

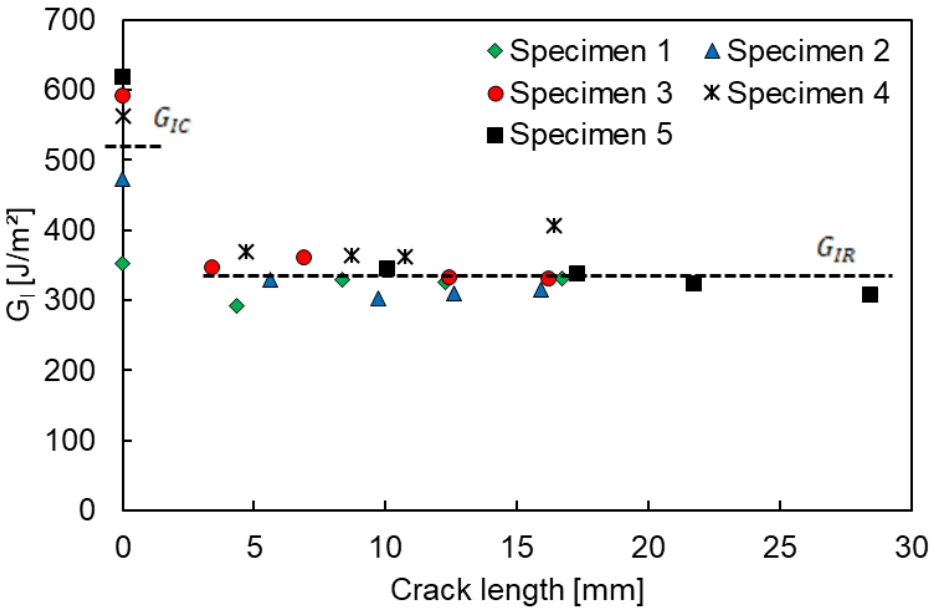

Fig. 2.4 Mode I fracture toughness G_I – crack length relationship for all specimens. Dotted lines show the average G_I values.

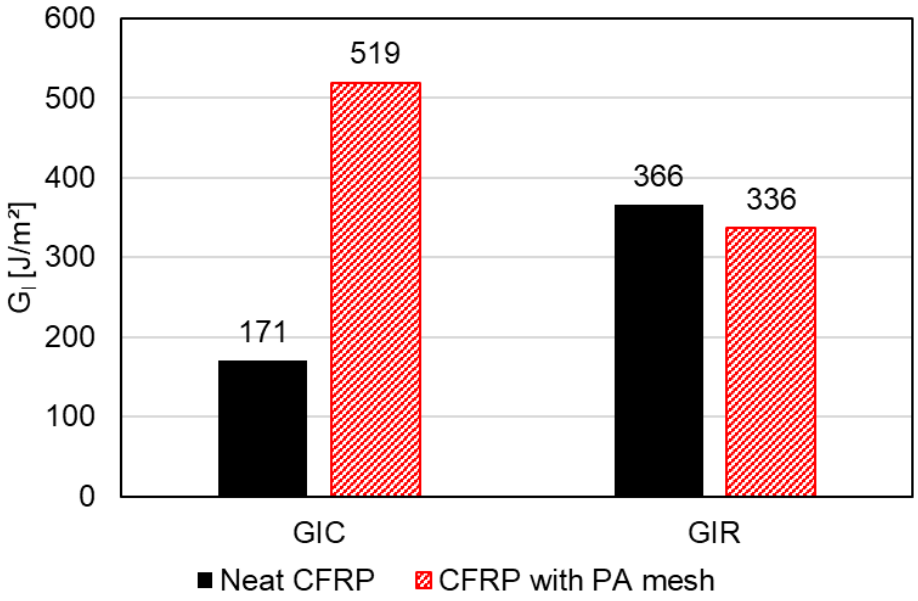

Fig. 2.5 Comparison of mode I interlaminar fracture toughness between neat CFRP laminate and CFRP laminate with PA mesh insert.

2.2 Mode II fracture toughness evaluation (End Notched Flexure (ENF) test)

To obtain the Mode II interlaminar fracture toughness value, the End Notched Flexure (ENF) tests were conducted. Details regarding the specimen dimensions, test procedure, and calculation method for the Mode II interlaminar fracture toughness value are described below.

2.2.1 Materials and specimen manufacturing

The materials used for specimen manufacturing in the ENF test are identical to those used in the DCB tests, as outlined in section 2.1.1. In this case, the laminates are cut into the measurements illustrated in Fig. 2.6 and detailed in Table 2.3. The edges of the specimens manufactured were then polished using a same polishing technique described in section 2.1.1.

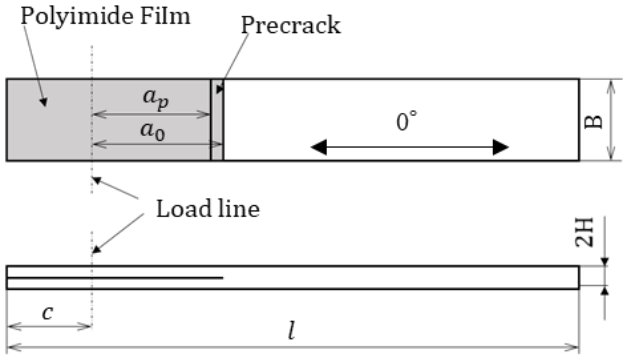

Fig. 2.6 Schematic specimen configuration for ENF test.

Table 2.3 Specimen dimension for ENF test.

Symbol	Parts	Size [mm]
L	Length	110
$2H$	Thickness	2.3
B	Width	10
c	Distance from specimen end load line	20
a_p	Film crack length	25
a_0	Pre-crack length	31-35

2.2.2 ENF test method

Similar to DCB tests, ENF tests were carried out using a universal testing machine (SC-5H, JT Torsi Co.). In this study, measurements were taken of the load P and (maximum) deflection δ. Five specimens were tested. The load was applied at the midpoint of the support span with a distance of $2L$ = 70 mm, as shown in Fig. 2.7. The test speed was set at 0.5 mm/min.

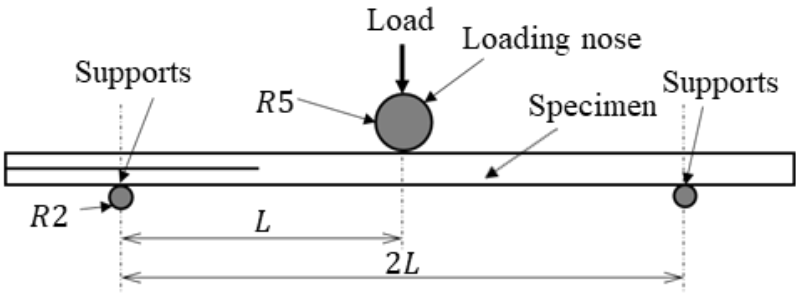

Fig. 2.7 Schematic for ENF test set up.

The mode II fracture toughness value G_{IIC} was calculated from Eqs. (2-2) and (2-3). In Eq. (2-2), a_1 represents an estimated value of crack length at a specific load, and a_1 was calculated from Eq. (2-3). Additionally, P_1 represents a specified load, C_0 denotes the compliance of the initial elastic part and C_1 represents the compliance at a specified load, calculated from the load-COD curve. The maximum load $P_{\max}$ was used as P_1 in this study.

$$G_{IIC} = \frac{9a_0^2 P_1^2 C_1}{2B(2L^3 + 3a_1^3)} \tag{2.2}$$

$$a_1 = \left[\frac{C_1}{C_0}a_0^3 + \frac{2}{3}\left(\frac{C_1}{C_0} - 1\right)L^3\right]^{\frac{1}{3}} \tag{2.3}$$

Fig. 2-8 illustrates the graph explaining C_1 and C_0.

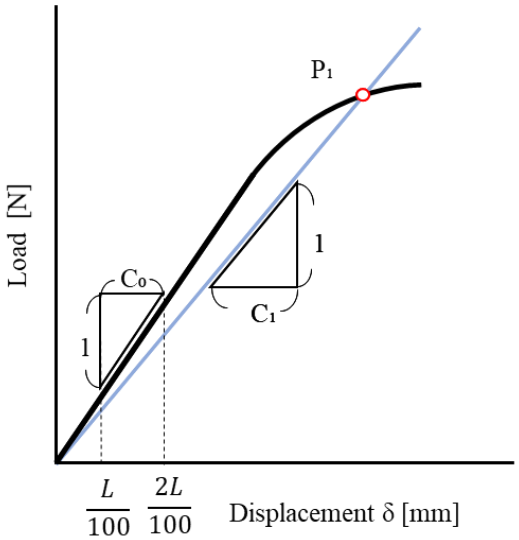

Fig. 2.8 Description of C_0 and C_1.

2.2.3 Results and discussion

Fig. 2.9 presents the load-deflection curves from the ENF test conducted on five specimens. The peak loads for each specimen are highlighted with red dots on the curves. Table

2.4 lists the maximum load values $P_1 = P_{\max}$, initial compliance in the elastic region C_0, initial crack length a_0, compliance at the maximum load C_1, estimated crack length at maximum load a_1, and the calculated mode II interlaminar fracture toughness G_{IIC} values for each specimen.

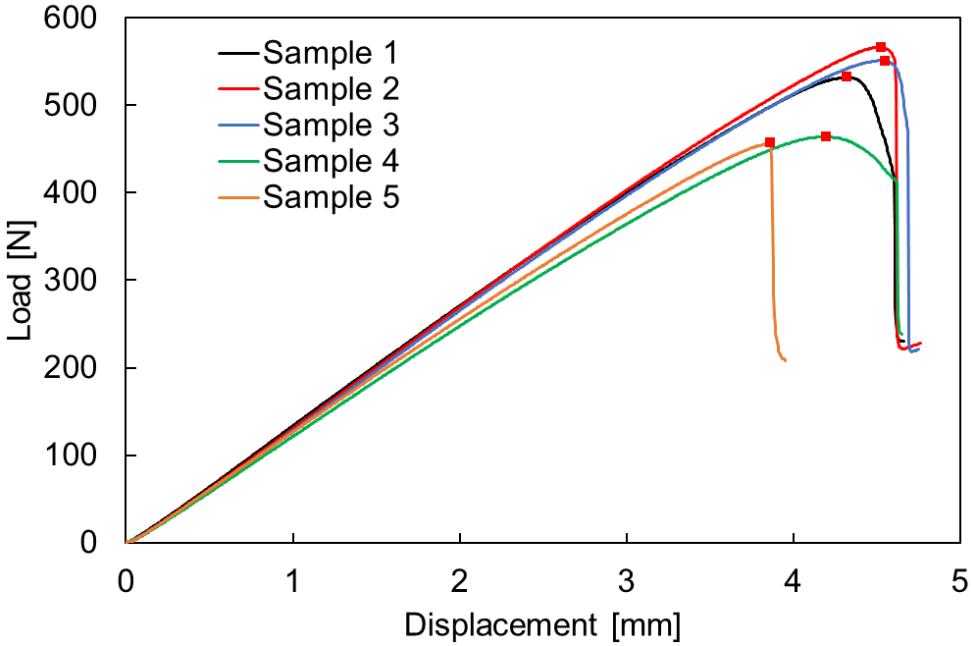

Fig. 2.9 Load – deflection curves from ENF tests. The red dots represent the maximum load point of each test.

Table 2.4 The measured and calculated parameters and mode II fracture toughness values G_{IIC}.

Specimen	Initial crack length a_0 [mm]	Compliance of the initial elastic part C_0 [m/N]	Estimated crack length a_1 [mm]	Compliance at the maximum load C_1 [m/N]	Maximum load $P_1 = P_{\max}$, [N]	G_{IIC} [J/m^2]
Specimen 1	12.9	0.007195	18.3	0.008123	532	3317
Specimen 2	11.3	0.007332	16.1	0.008002	566	3042
Specimen 3	13.1	0.007474	17.4	0.008220	551	3226
Specimen 4	16.5	0.007856	21.5	0.009138	464	3423
Specimen 5	15.5	0.007548	19.6	0.008454	457	2713
Average mode II fracture toughness value G_{IIC}						3144

Fig. 2.10 illustrates a comparison of the mode II fracture toughness G_{IIC}, values between CFRP laminates with and without PA mesh inserts. The displayed G_{IIC} values are averaged from five specimens tested. It is apparent that the CFRP laminates incorporating a PA mesh insert exhibit a mode II fracture toughness approximately three times greater than that of the neat laminates. This enhancement can be attributed to the integration of PA mesh within the CFRP layers, which absorbs the energy and altering the crack trajectory due to its microstructure, under shear stresses (mode II loading).

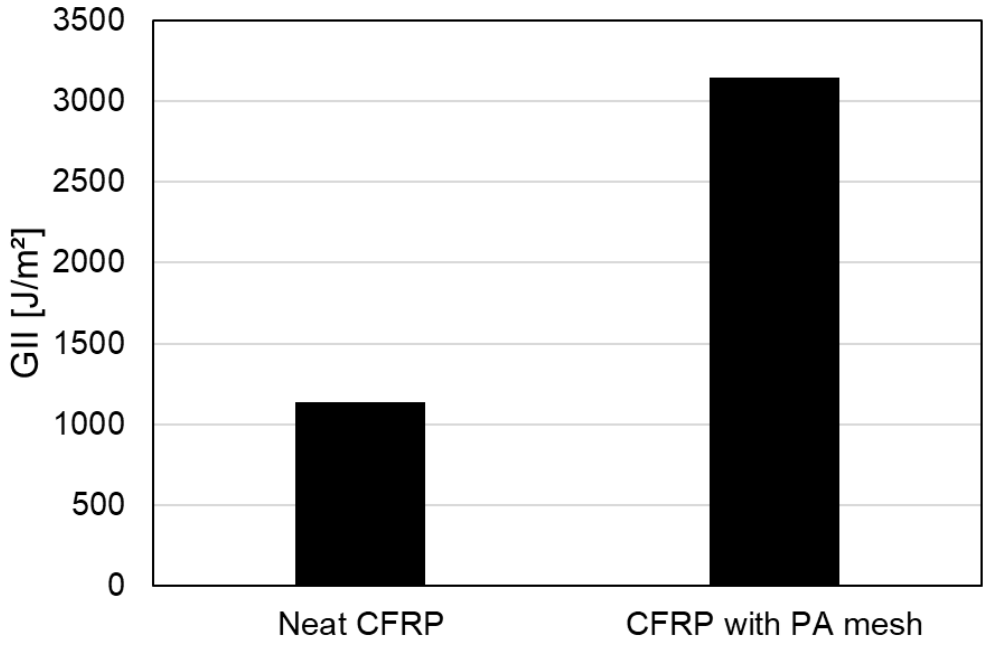

Fig. 2.10 Comparison of mode II interlaminar fracture toughness between neat CFRP laminate and CFRP laminate with PA mesh insert.

2.3 Conclusion

In conclusion, the study presents significant findings on the interlaminar fracture toughness of CFRP laminates, analyzing both Mode I and Mode II loading conditions. For Mode I, the investigation highlights that the inclusion of PA mesh in CFRP laminates substantially enhances the critical strain energy release rate (G_{IC}), with values approximately three times higher than those of neat laminates. However, the propagation strain energy release rate (G_{IR}) indicates a reduced capacity to hinder crack propagation once initiated, suggesting that the current configurations of PA mesh are not optimized for the best performance under Mode I loading. This underscores the necessity for a structured investigation into the PA mesh dimensions and configurations, proposing future studies that involve a factorial design experiment to optimize these variables for enhanced fracture toughness. For Mode II, the presence of PA mesh in CFRP laminates yields a notable improvement in fracture toughness, with the G_{IIC} values being significantly higher compared to neat laminates. This enhancement is attributed to the mesh's ability to disrupt and alter the crack propagation path, necessitating additional energy for progression and effectively enhancing the laminate's resistance to shear-induced delamination.

The total sum of the improvements in G_{IC} and G_{IIC} values suggests that CFRP laminates with PA mesh inserts markedly outperform their neat counterparts in handling diverse loading conditions. This result underscores the potential of PA mesh as a critical component in the design of advanced composite materials, aiming for higher durability and better performance in critical applications. Future research should continue to refine the mesh configurations to maximize these benefits across different modes of fracture, ensuring optimal performance and extended usability of CFRP structures.

Chapter 3

Application of PA mesh in CFRP laminates with ply discontinuities

To confirm the suppression of interlaminar delamination by inserting PA mesh in CFRP laminates, unidirectional (UD) CFRP laminates with ply discontinuities were used. The tensile testing methods, results, and discussions for this structure are described in this chapter.

3.1 Materials and specimen manufacturing

The laminate configuration of the specimens used in the uniaxial tensile test was $[0_2/PA/0_2]s$. Initially, as illustrated in Fig. 3.1, a stack of four plies of carbon fiber/epoxy UD tape prepreg (Torayca, T700SC/2592), each with a thickness of 0.14 mm, was bisected perpendicularly to the fiber direction into two equal halves. These halves were then aligned with a predefined gap to form a symmetrical laminate structure, with two PA meshes and continuous $[0]_2$ UD laminates attached above and below the gap. The gap or resin pocket length L_0 was set to approximately 1 mm. In this study, the specimens were manufactured with a 20 mm PA mesh embedded and with PA mesh fully embedded throughout their entire structure. A schematic diagram of the structures is shown in Fig. 3.2. The PA mesh used in this study has a fiber diameter of 50 µm, a thickness of 87 µm, and an opening of 95 µm (N-NO175T, NBC Meshtec Inc.). The laminate was then cured using autoclave molding at a temperature of 130°C and a pressure of 0.2 MPa. During the curing process, the elevated temperature caused the epoxy resin in its gel-phase condition from the adjacent UD plies to flow into the gap, forming a resin pocket. This resin pocket then cured simultaneously with the rest of the laminate. After cooling to room temperature, the laminates were sectioned into specimens as depicted in Fig. 3.3.

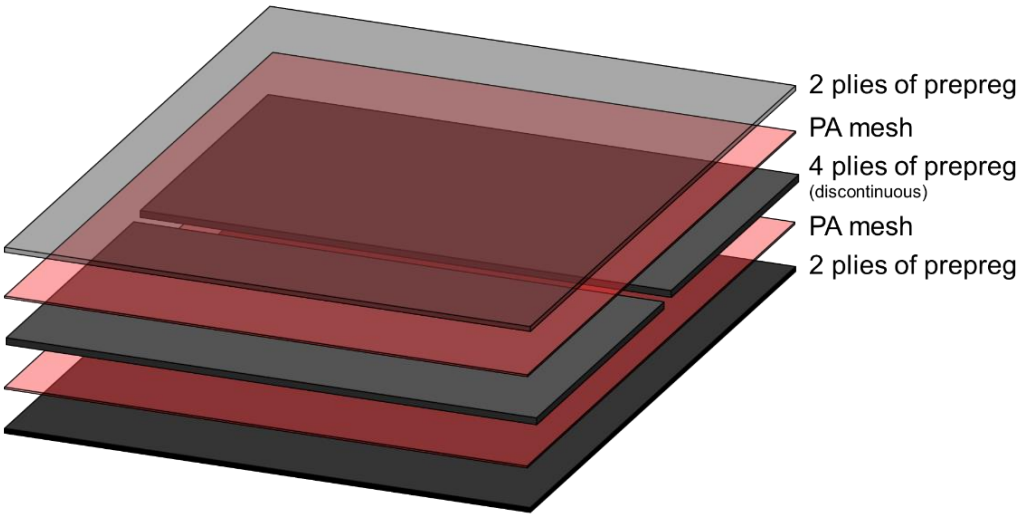

Fig. 3.1 Illustration of laminate with discontinuous plies and PA mesh embedded.

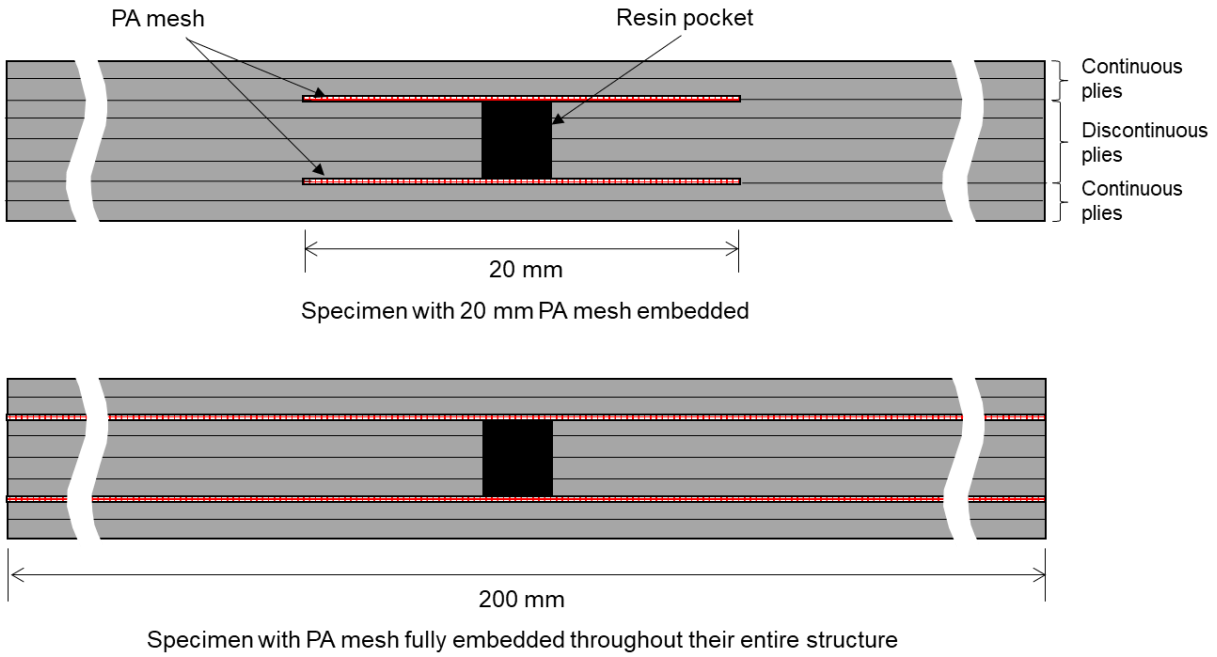

Fig. 3.2 Placement of PA mesh in the specimen.

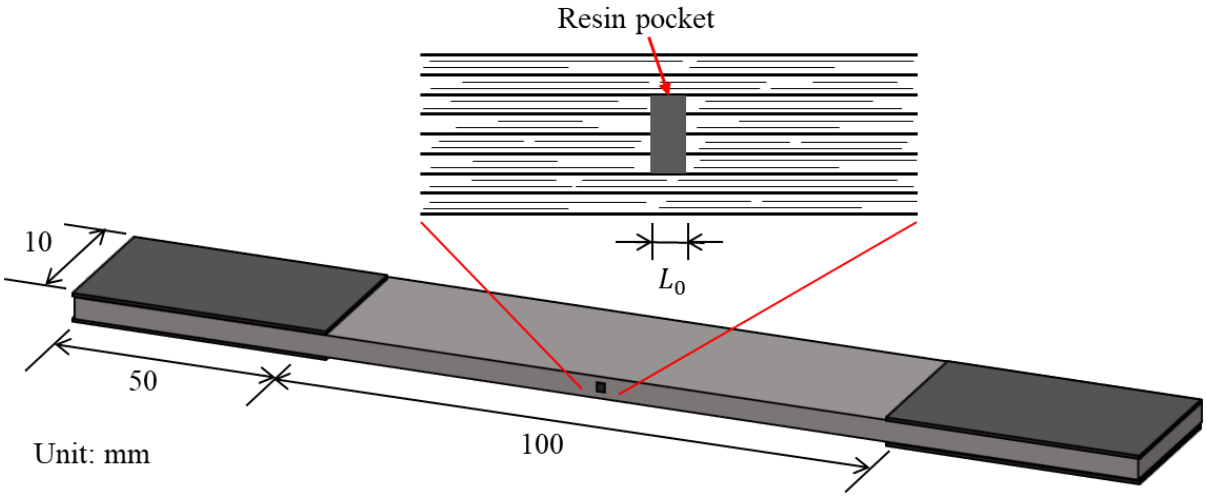

Fig. 3.3 Specimen measurement.

3.2 Tensile test and damage evaluation methods

Monotonic tensile loading was subsequently applied at a crosshead speed of 0.5 mm/min using a TENSILON RTF-1350 tensile testing machine. To measure the strain, two strain gauges, each with a gauge length of 5 mm (KFGS-5-120-C1-11L1M2R, Kyowa), were utilized. As shown in Fig. 3.4, one strain gauge was adhered directly above the ply discontinuity area (resin pocket) and another was affixed 20 mm away from the center of the resin pocket to measure the laminate's strain without significant influence from the resin pocket. In-situ edge observations were performed using a KEYENCE VHX-1000 optical microscope (lens: MX 7575CS) to verify the presence of the damages.

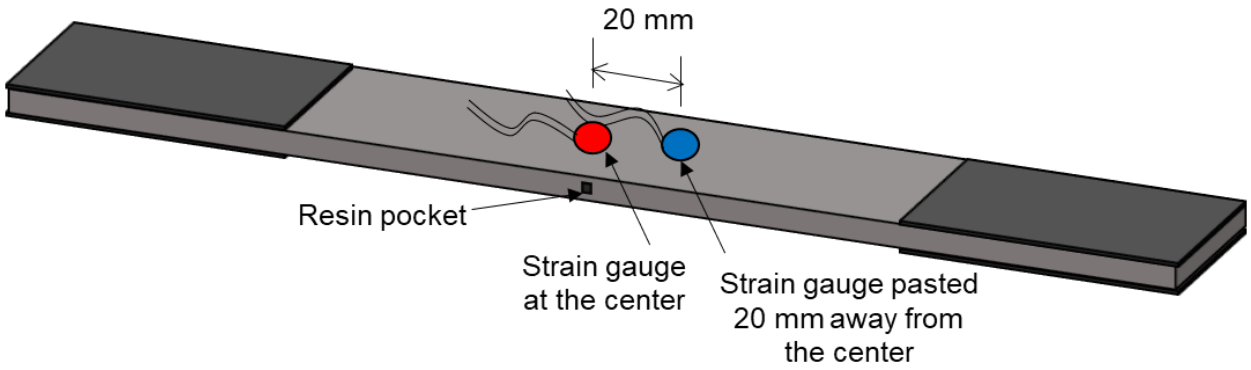

Fig. 3.4 Strain gauge placement on a specimen.

3.3 Results and discussion

3.3.1 CFRP laminate with no PA mesh embedded (neat CFRP)

To confirm the suppression of interlaminar delamination by embedding the PA mesh, a tensile test was also conducted on neat CFRP specimens (specimens without the insertion of PA mesh) for comparison purposes. The stress-strain diagram from the tensile test is shown in Fig. 3.5. Additionally, the microscopic edge observation during the test is shown in Fig. 3.6. The results for the CFRP specimens with no PA mesh embedded were referenced from previous research (Fikry, 2022).

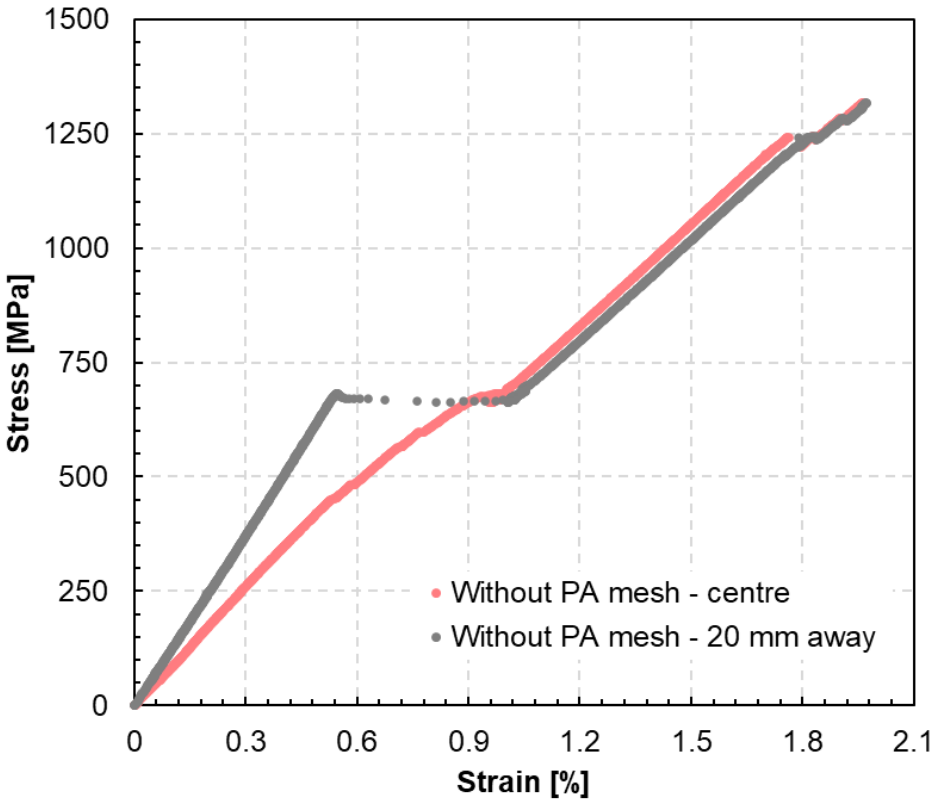

Fig. 3.5 Stress-strain curves from the tensile test of a specimen with no PA mesh embedded (Fikry, 2022).

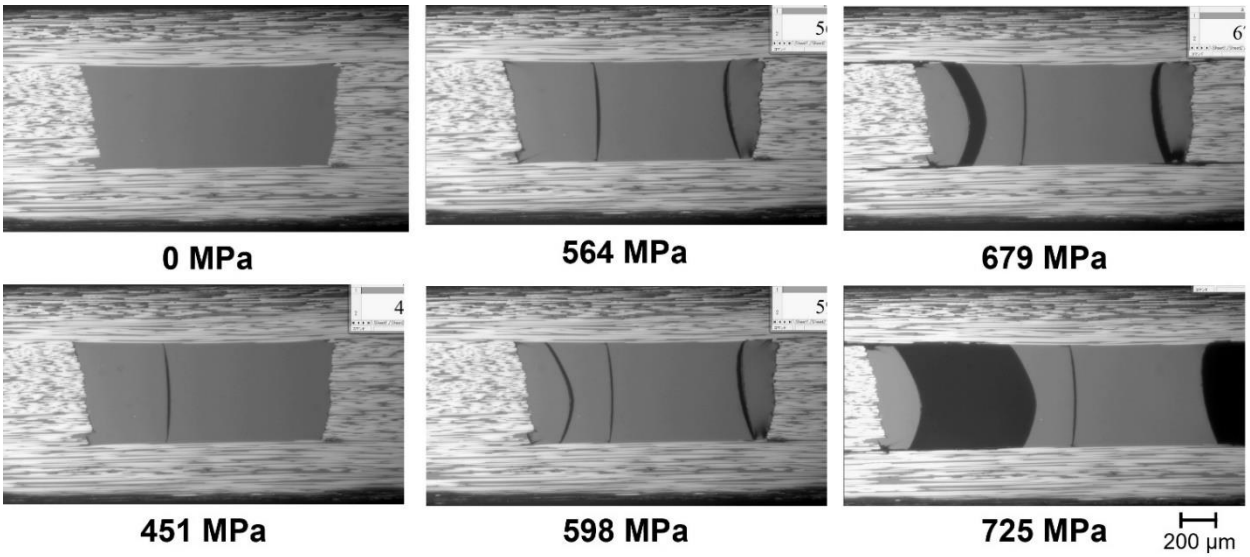

Fig. 3.5 Results of edge observations (around the resin pocket area) at specific applied stress levels for a specimen with no PA mesh embedded (Fikry, 2022).

From the nonlinearity (strain jump) of the stress-strain curve in Fig. 3.6 and the edge observation in Fig. 3.6, it is observed that an initial crack occurred at 451 MPa during the test. The second matrix crack in the resin pocket occurred at 564 MPa, and delamination was found to initiate from the crack tip at this stress level. The third matrix crack occurred at 679 MPa. In addition to the edge observation, the propagation of delamination can also be confirmed by the decrease in the gradient of the stress-strain curve, which was recorded by the strain gauge pasted at the center, after the initiation of the matrix crack. Furthermore, the stress-strain diagram indicates that complete delamination occurred at approximately 725 MPa for this specimen.

3.3.2 CFRP laminate with 20 mm PA mesh embedded

The results of the uniaxial tensile test for specimens with 20 mm PA mesh inserts and neat CFRP specimens were compared. The stress-strain curves for both strain gauges (center and 20 mm away) are shown in Fig. 3.6(a), and the stress-strain curves comparing the PA specimen to the neat CFRP specimen are shown in Fig. 3.6(b). Additionally, Fig. 3.7 presents the stress-strain curves and results of edge observations (around the resin pocket area) at specific applied stress levels for a specimen with a 20 mm PA mesh embedded. The edge observation images were captured from a video recorded by the microscope.

Furthermore, Fig. 3.8, Fig. 3.9, and Fig. 3.10 show the results of edge observations during the tensile test of a laminate with a 20 mm PA mesh embedded, around the resin pocket area, to the left, and to the right of the resin pocket area, respectively. Stress levels applied are labeled below each image. In each figure, (a) shows the observations without damage highlights, and (b) shows the observations with damage highlighted in red.

The stress-strain diagrams in Fig. 3.6(b) show that, compared to neat CFRP specimens, the initial stress-strain curve slope for specimens with PA mesh inserts, as measured by the strain gauge pasted at the center, did not exhibit significant differences. However, for the strain gauge pasted 20 mm away, the initial gradient was lower than that of the neat CFRP specimen. This

indicates that the stiffness was affected by the presence of the embedded PA mesh, causing some stress concentration at the material's terminal (tapered part).

The first matrix crack in the resin pocket occurred at 456 MPa, while the second one occurred at 520 MPa. Small delaminations from the matrix crack tips started to occur at 617 MPa, but the propagation of delamination is very slow as the applied stress increases. After 600 MPa, while the slope of the curve for the neat CFRP specimen tended to decrease, the slope for the specimens with PA mesh inserts remained almost unchanged, showing linear behavior up to high stress levels. In other words, for neat CFRP specimens, delamination progressed significantly after 600 MPa, whereas for specimens with PA mesh inserts, delamination progressed slowly within the mesh layer up to high stress levels.

There is a large strain jump at approximately 720 MPa for the strain gauge pasted at the center, indicating a sudden delamination at all four edges of the resin pocket. Even though it is not yet a complete delamination at this point, the load continues to increase and delamination progresses slowly until a very high stress level of 1121 MPa. Complete delamination (ply separation) between the continuous and discontinuous plies occurs at this stress level, leading to complete fracture soon after. This stress level for ply separation and subsequent fracture is significantly higher compared to the neat CFRP specimen, where complete delamination occurred at approximately 725 MPa. This can be confirmed by looking at the edge observation results in Fig. 3.7 to 3.10.

This substantial enhancement can be attributed to the integration of PA mesh within the CFRP layers, which effectively interrupts the natural crack propagation path. The mesh's structural characteristics alter the crack trajectory, requiring additional energy for crack progression and thereby significantly increasing the interlaminar fracture toughness. From these observations, it can be confirmed that inserting PA mesh into CFRP laminates increases interlaminar fracture toughness and is effective in suppressing delamination in CFRP laminates with discontinuities.

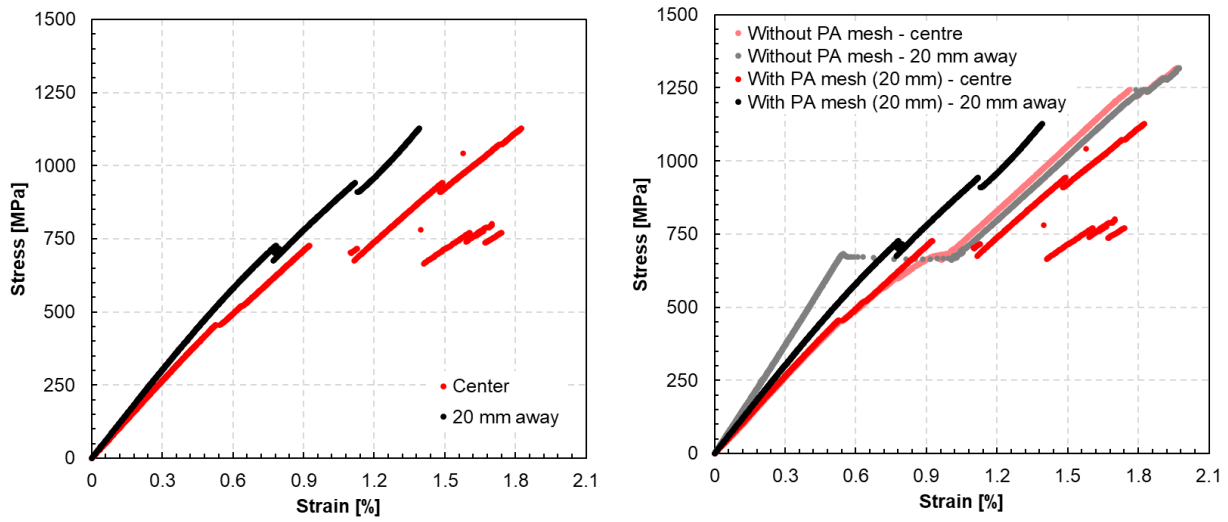

(a) Stress-strain curves for both strain gauges (center and 20 mm away)

(b) Stress-strain curves with comparison to neat CFRP specimen

Fig. 3.6 Stress-strain curves from the tensile test of a specimen with a 20 mm PA mesh embedded.

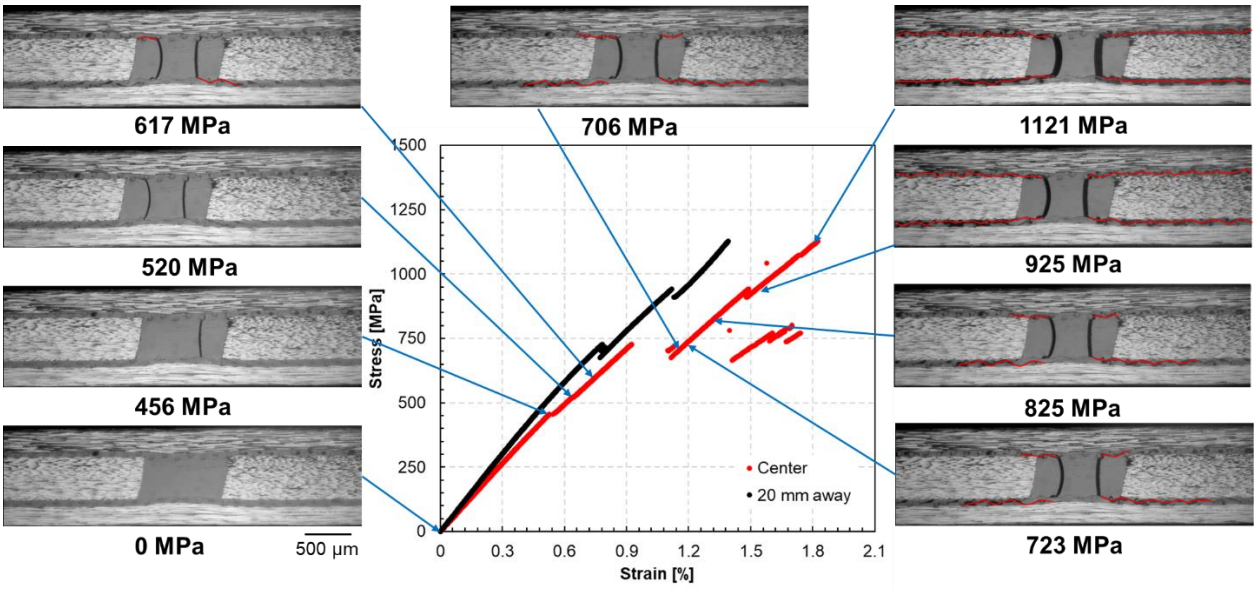

Fig. 3.7 Stress-strain curves and results of edge observations (around the resin pocket area) at specific applied stress levels for a specimen with a 20 mm PA mesh embedded.

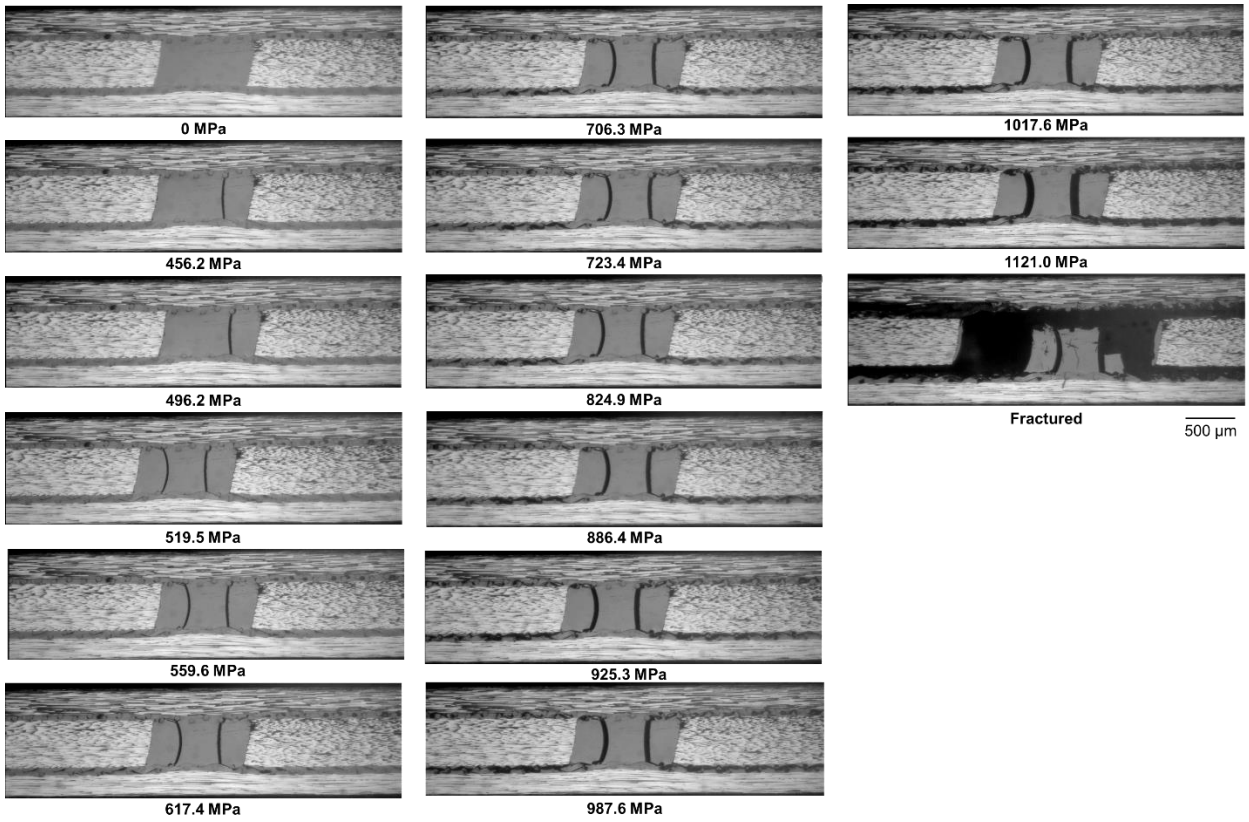

(a) Without damage highlights

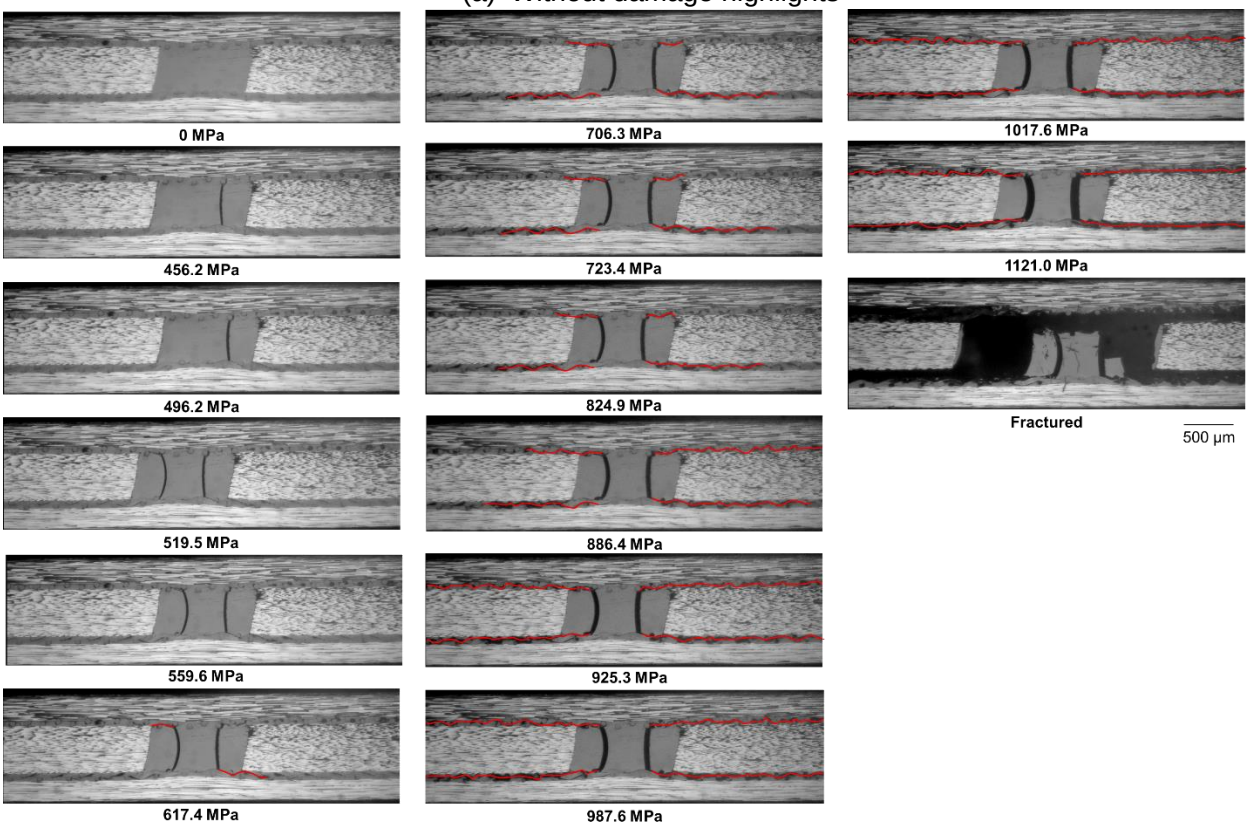

(b) With damage highlights

Fig. 3.8 Results of edge observations (around the resin pocket area) during the tensile test of a laminate with a 20 mm PA mesh embedded. Stress levels applied are labeled below each image.

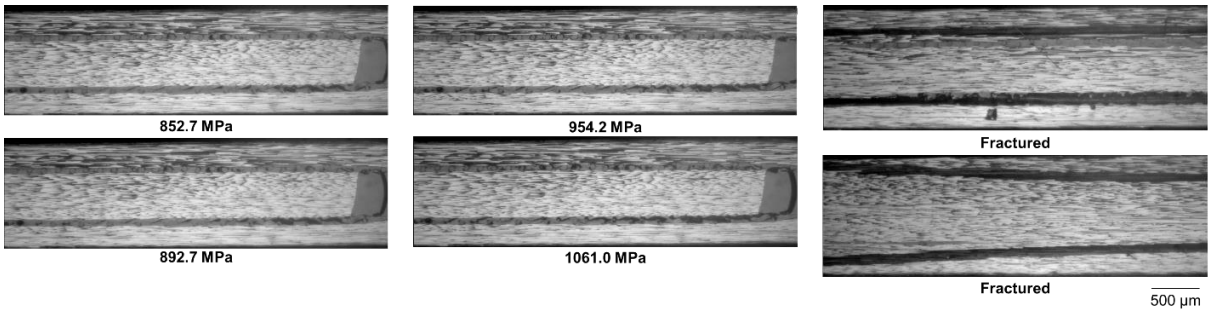

(a) Without damage highlights

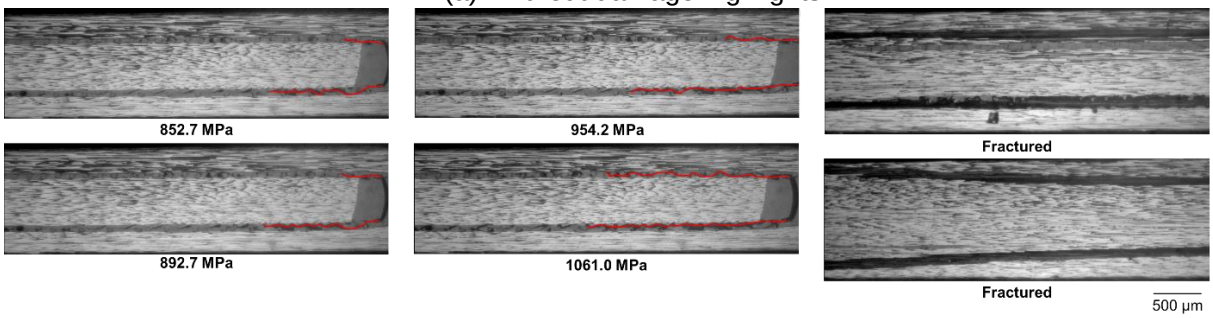

(b) With damage highlights

Fig. 3.9 Results of edge observations (to the left of the resin pocket area) during the tensile test of a laminate with a 20 mm PA mesh embedded. Stress levels applied are labeled below each image.

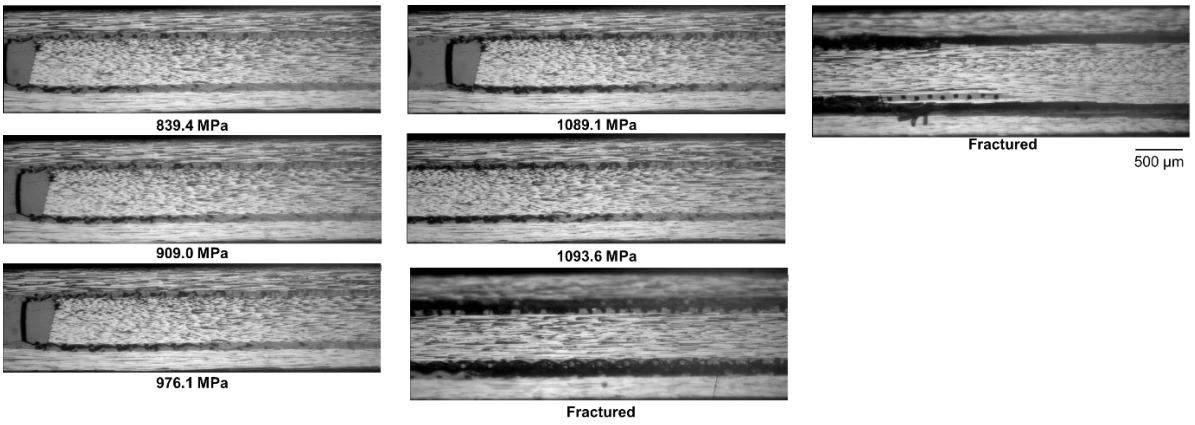

(a) Without damage highlights

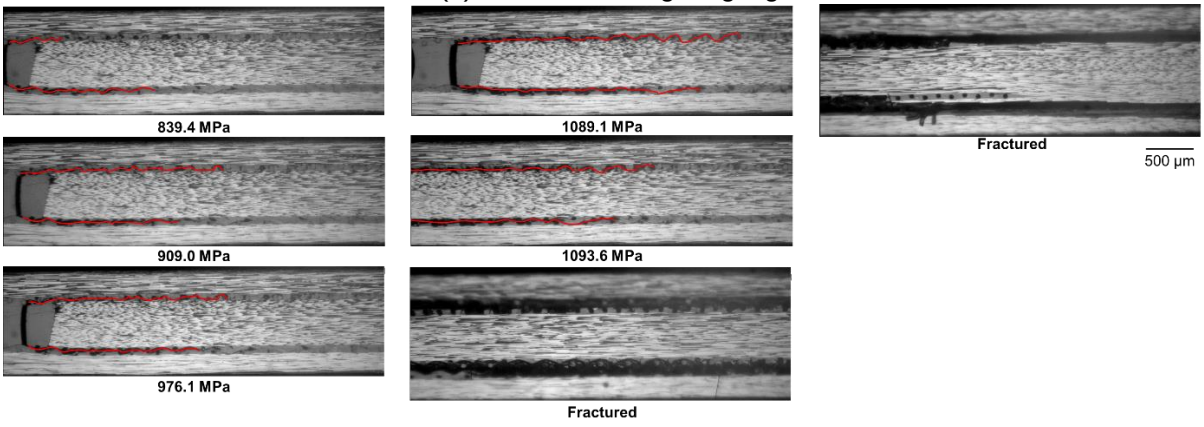

(b) With damage highlights

Fig. 3.10 Results of edge observations (to the right of the resin pocket area) during the tensile test of a laminate with a 20 mm PA mesh embedded. Stress levels applied are labeled below each image.

3.3.3 CFRP laminate with a PA mesh fully embedded throughout its entire structure

The results of the uniaxial tensile test for laminates with a PA mesh fully embedded throughout their entire structure and neat CFRP specimens were compared. The stress-strain curves for both strain gauges (center and 20 mm away) are shown in Fig. 3.11(a), and the stress-strain curves comparing the PA specimen to the neat CFRP specimen are shown in Fig. 3.11(b). Additionally, Fig. 3.12 presents the stress-strain curves and results of edge observations (around the resin pocket area) at specific applied stress levels for a laminate with a PA mesh fully embedded throughout its entire structure. The edge observation images were captured from a video recorded by the microscope.

Furthermore, Fig. 3.13, Fig. 3.14, and Fig. 3.15 show the results of edge observations during the tensile test of a laminate with a PA mesh fully embedded throughout its entire structure, around the resin pocket area, to the left, and to the right of the resin pocket area, respectively. Stress levels applied are labeled below each image. In each figure, (a) shows the observations without damage highlights, and (b) shows the observations with damage highlighted in red.

The stress-strain diagrams in Fig. 3.11(b) show that, compared to neat CFRP specimens, the initial stress-strain curve slope for specimens with PA mesh inserts, as measured by both the strain gauge pasted at the center and the strain gauge pasted 20 mm away, did not exhibit significant differences. This indicates that the PA mesh is continuous, so there is no PA mesh material discontinuity in the laminate that caused stress concentration in the laminate, except around the resin pocket area. Thus, the strain value measured by the strain gauge pasted 20 mm away from the center was not affected. As the strain was measured on the outer surface of the specimen (CFRP part), the strain behaves as in the neat CFRP specimen even though there is PA mesh embedded inside.

The first matrix crack in the resin pocket occurred at 396 MPa, which is not very different from the neat CFRP specimen. The second matrix crack occurred at 1286 MPa, which is different from the neat CFRP specimen and the specimen with a 20 mm PA mesh embedded. In these cases, the second crack usually occurred soon after the first one, and after that, delamination started to propagate. However, in the specimen with the PA mesh fully embedded, the second crack occurred after significant delamination propagation.

After 600 MPa, while the slope of the curve for the neat CFRP specimen tended to decrease, the slope for the specimens with PA mesh inserts remained almost unchanged, showing linear behavior up to high stress levels. In other words, for neat CFRP specimens, delamination progressed significantly after 600 MPa, whereas for specimens with PA mesh inserts, delamination progressed slowly within the mesh layer up to high stress levels.

Delamination starts to appear in the edge observations at 780 MPa and progresses slowly as the applied stress increases. Additionally, at 1153 MPa, delamination also propagated between the continuous plies. This might occur because the interlaminar toughness between the continuous and discontinuous plies is enhanced by the embedded PA mesh, causing the crack to propagate in locations where the fracture toughness is lower. The delamination between the continuous plies continues to occur as the applied stress increases, as can be observed in Fig. 3.13 at applied stress levels of 1286 and 1390 MPa. Since delamination propagates very slowly in the specimen, it fractured right after the complete ply separation at 1390 MPa.

In this case, there is no large strain jump, and the linearity of the stress-strain curves continues until a very high stress level of 1390 MPa. This can be confirmed by looking at the edge observation results in Fig. 3.12 to 3.15. This improvement can be attributed to the integration of PA mesh within the CFRP layers, which absorbs energy and alters the crack trajectory due to its microstructure. Additionally, even with the PA mesh embedded, the strength of the material is not affected, and the fractured stress and strain remain the same as for the neat CFRP laminate.

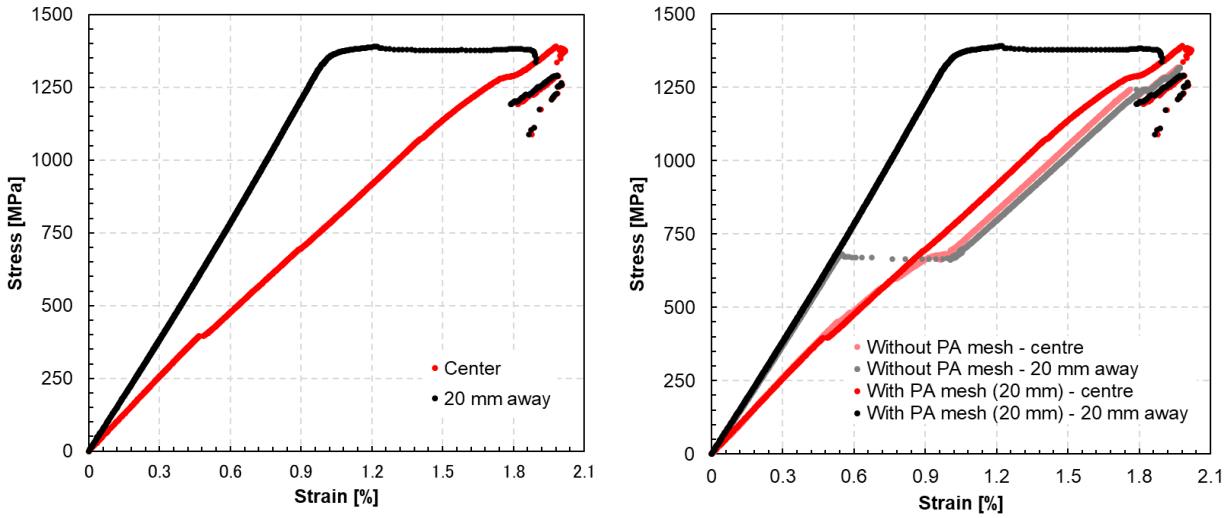

(a) Stress-strain curves for both strain gauges (center and 20 mm away)

(b) Stress-strain curves with comparison to specimen without inserted PA mesh interlayer

Fig. 3.11 Stress-strain curves from the tensile test of a specimen with PA mesh fully embedded throughout its entire structure.

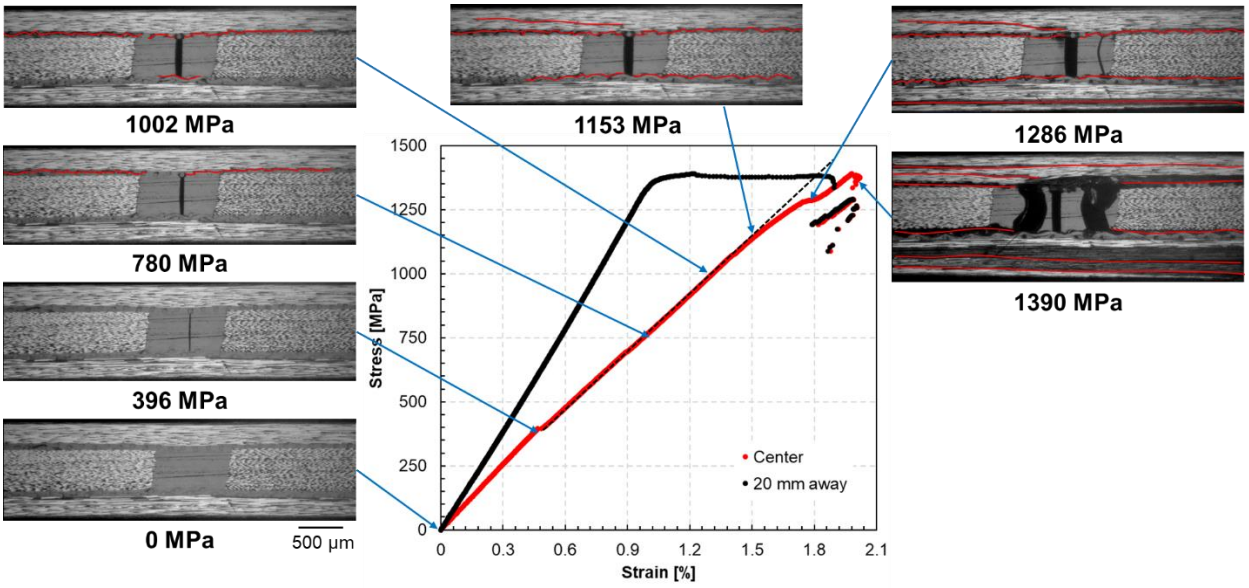

Fig. 3.12 Stress-strain curves and results of edge observations at specific applied stress levels for a specimen with a PA mesh fully embedded throughout its entire structure.

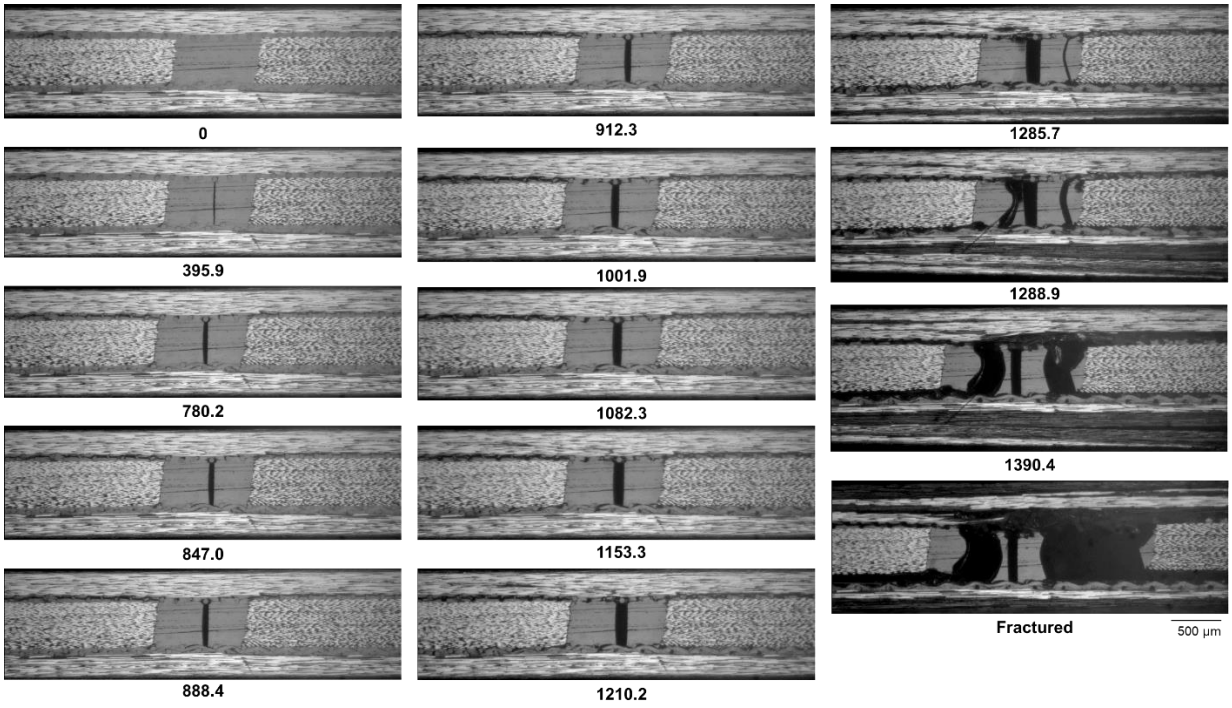

(a) Without damage highlights

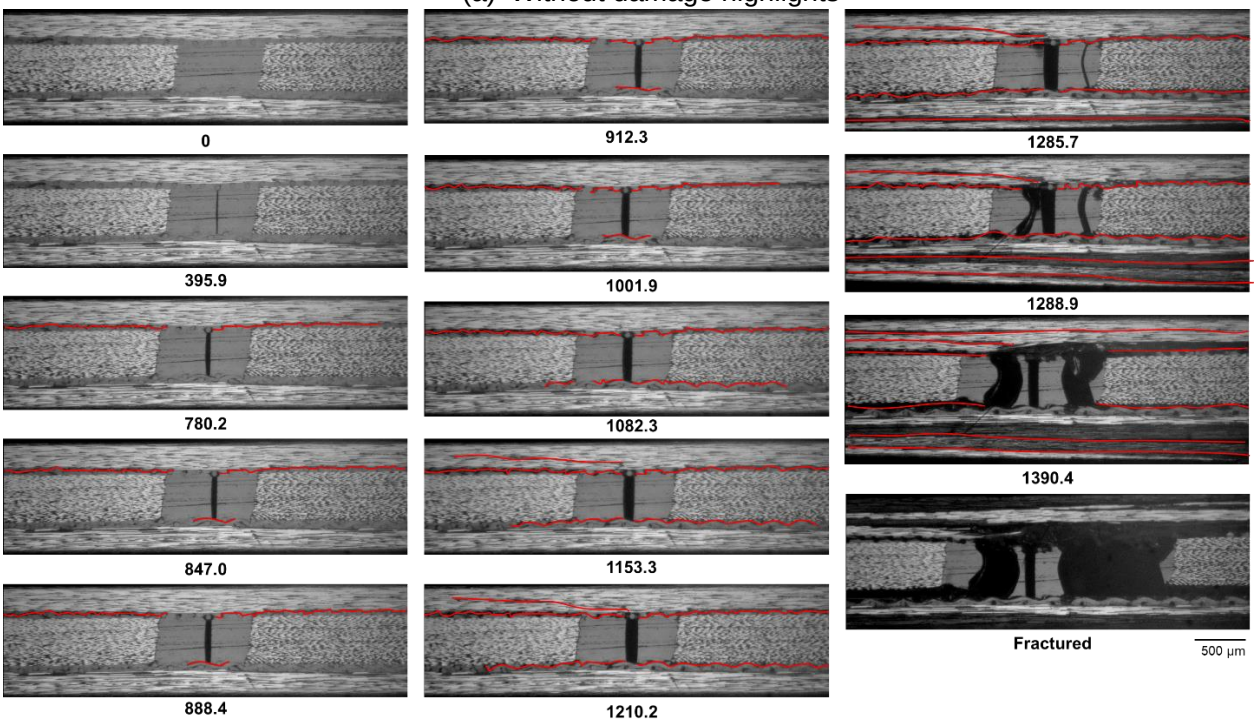

(b) With damage highlights

Fig. 3.13 Results of edge observations (around the resin pocket area) during the tensile test of a specimen with a PA mesh fully embedded throughout its entire structure. Stress levels applied are labeled below each image.

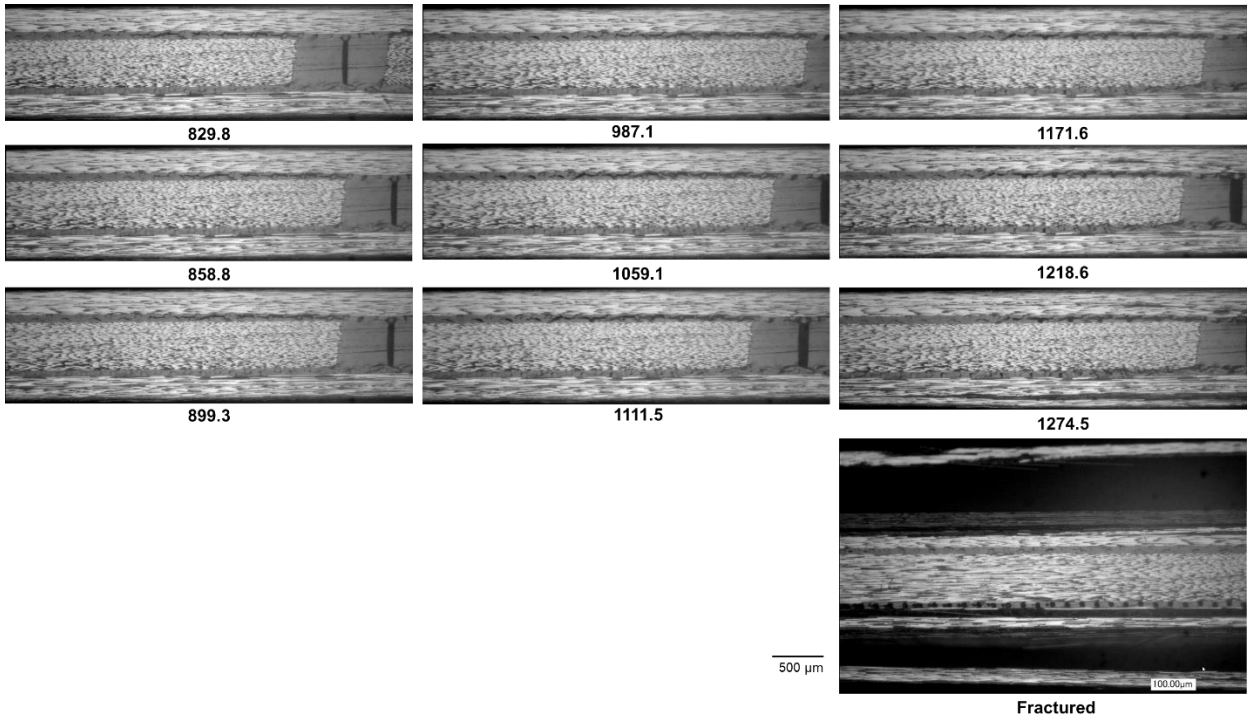

(a) Without damage highlights

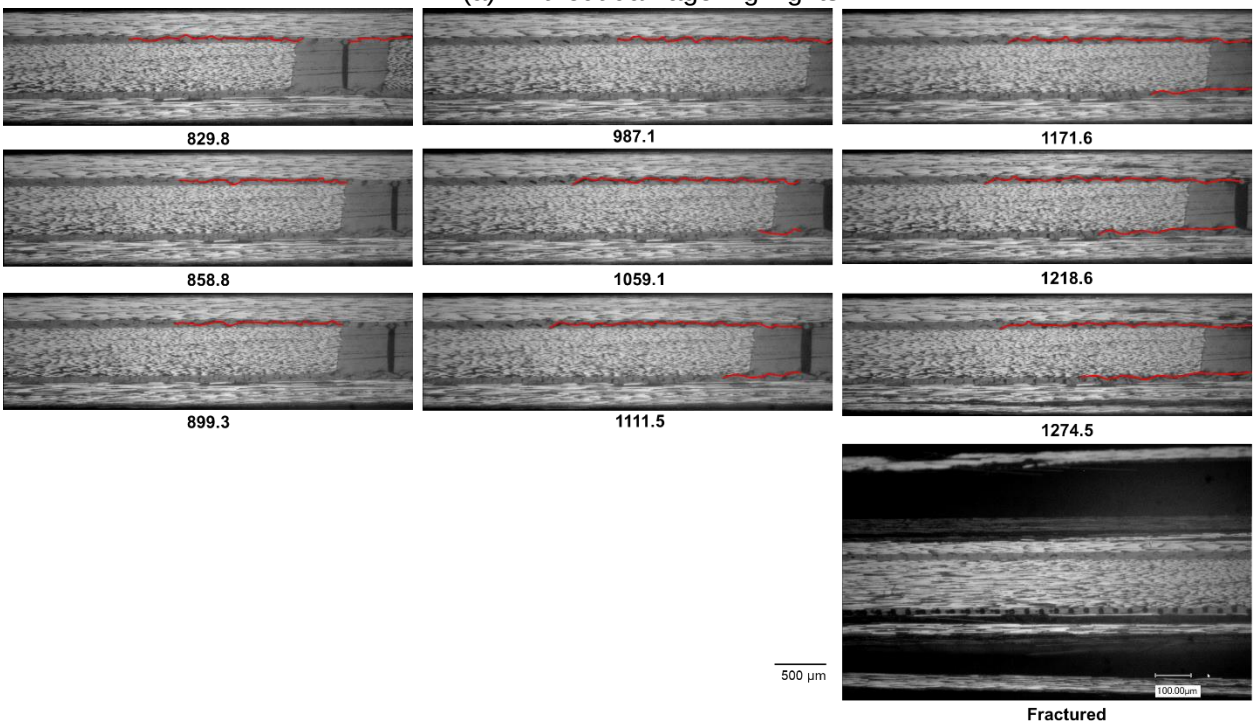

(b) With damage highlights

Fig. 3.14 Results of edge observations (to the left of the resin pocket area) during the tensile test of a specimen with a PA mesh fully embedded throughout its entire structure. Stress levels applied are labeled below each image.

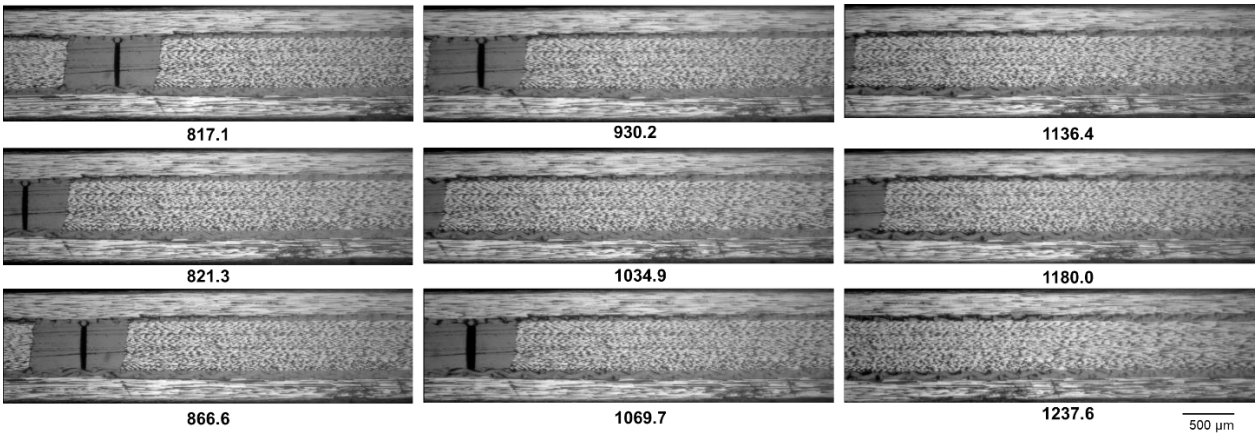

(a) Without damage highlights

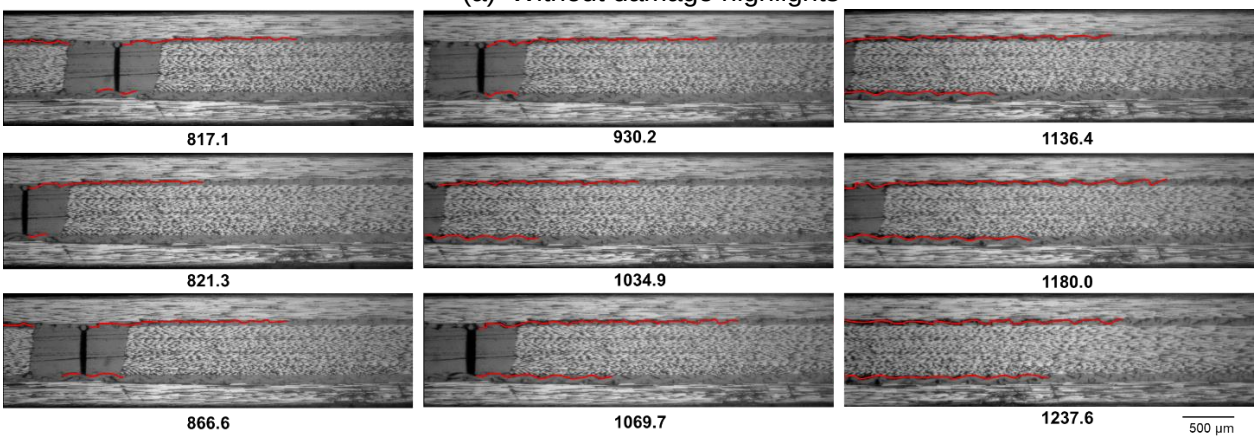

(b) With damage highlights

Fig. 3.15 Results of edge observations (to the right of the resin pocket area) during the tensile test of a specimen with a PA mesh fully embedded throughout its entire structure. Stress levels applied are labeled below each image.

3.4 Conclusion

Comparing the neat CFRP laminate and the CFRP laminates with PA mesh inserts, both the initial stress-strain curve slopes and the behavior of the laminates under stress reveal significant differences. For neat CFRP specimens, delamination begins after the initial matrix crack and progresses rapidly, leading to a noticeable decrease in the slope of the stress-strain curve. In contrast, the presence of PA mesh, whether in a 20 mm section or fully embedded throughout the laminate, alters the delamination behavior. For specimens with PA mesh, the initial stress-strain curve slope remains largely unchanged, and delamination progresses much more slowly, indicating improved resistance to crack propagation.

The fully embedded PA mesh laminate demonstrates superior performance in suppressing delamination compared to both neat CFRP and the 20 mm PA mesh insert. Delamination in this case is delayed and progresses very slowly, even at higher stress levels. Additionally, the strength of the material, as indicated by the fractured stress and strain, remains unaffected by the PA mesh, maintaining the same levels as the neat CFRP laminate.

This substantial enhancement in suppressing delamination can be attributed to the integration of PA mesh within the CFRP layers, which effectively absorb the energy, thus interrupts the natural crack propagation path. The mesh's structural characteristics alter the crack

trajectory, requiring additional energy for crack progression and thereby significantly increasing the interlaminar fracture toughness. By interrupting the crack path, the PA mesh forces the crack to navigate a more complex route, distributing the stress and slowing the progression of delamination. This mechanism not only improves the interlaminar fracture toughness but also maintains the structural integrity and strength of the CFRP laminate, making the fully embedded PA mesh configuration the most effective for enhancing the performance of CFRP laminates.

However, the results in this study might not yet show the optimum outcome for delamination suppression. As explained in Chapter 2, the propagation strain energy release rate (G_{IR}) for mode I interlaminar fracture toughness indicates a reduced capacity to hinder crack propagation once initiated, suggesting that the current configurations of PA mesh are not optimized for the best performance under mode I loading. This underscores the necessity for a structured investigation into the PA mesh dimensions and configurations. Future studies should involve a factorial design experiment to optimize these variables for enhanced fracture toughness, ensuring that the benefits observed with the fully embedded PA mesh are maximized.

Acknowledgement

I extend my deepest gratitude to Prof. Shinji Ogihara for his supervision and advice throughout the research. His expertise and guidance have been instrumental in navigating the complexities of the study. I also wish to thank Associate Professor Hayato Nakatani at the Osaka Metropolitan University in the Graduate School of Engineering, Division of Mechanical Engineering, and the School of Engineering, Department of Mechanical Engineering, for his invaluable advice on the research and for generously providing the PA mesh materials used in this study.

This work was supported by JKA and its promotion funds from KEIRIN RACE. We are immensely thankful for their financial and material support, which greatly facilitated the progress and completion of this research.

References

Bonfilt, "Flour Mill Mesh for Plansifter Screen | Nylon & Polyester Sieve Bolting Cloth," available at: https://www.bonfilt.com/product/mill-mesh/, Accessed April 2024.

Fikry, M.J., Ogihara, S., & Vinogradov, V. "The effect of matrix cracking on mechanical properties in fiber-reinforced polymers laminates," Mechanics of Advanced Materials and Modern Processes, Vol. 4, Issue 3, 2018, pp. 1-16.

Fikry, M.J., Vinogradov, V., & Ogihara, S. "Experimental observation and modeling of resin pocket cracking in unidirectional laminates with ply discontinuity," Composites Science and Technology, Vol. 218, 2022, p. 109175.

Forster, E., Clay, S., Holzwarth, R., & Paul, D. "Flight vehicle composite structures," in the 26th Congress of the International Council of the Aeronautical Sciences and 8th AIAA Aviation Technology, Integration, and Operations Conference, 2008, p. 8976.

Huang, T., & Bobyr, M. "A Review of Delamination Damage of Composite Materials," Journal of Composites Science, Vol. 7, Issue 11, 2023, p. 468.

Jason Mills LLC, "Nylon & Polyester Mesh Screen Filters," available at: https://www.jasonmills.com/blog/nylon-polyester-mesh-filters/, Accessed April 2024.

NASA - Durability, Damage Tolerance, and Reliability Branch, "Damage Mechanics of Composite Materials," available at: https://ddtrb.larc.nasa.gov/composites/, Accessed April 2024.

Ou, Y., Fu, A., Wu, L., Yi, X., & Mao, D. "Enhanced interlaminar fracture toughness of unidirectional CFRP laminates with tailored microstructural heterogeneity of toughening layer," Composites Part A: Applied Science and Manufacturing, Vol. 176, 2024, p. 107872.

Richard, H.A., & Sander, M. "Fundamentals of Fracture Mechanics," in Fatigue Crack Growth, Solid Mechanics and Its Applications, Vol. 227, Springer, 2016, p. various.

Simon, I., & Banks-Sills, L. "Mixed mode I/II interlaminar initiation fracture toughness of a secondary bonded pultrusion composite laminate," Theoretical and Applied Fracture Mechanics, Vol. 114, 2021, p. 103018.

Song, W., Chen, Y., Mu, Z., Wang, Y., Zhang, Z., Wang, Z., Liu, L., Zhang, B., Li, Y., Li, B., Zhang, D., Zhang, J., Niu, S., Han, Z., & Ren, L. "A feather-inspired interleaf for enhanced interlaminar fracture toughness of carbon fiber reinforced polymer composites," Composites Part B: Engineering, Vol. 236, 2022, p. 109827.

Sun, X., Liu, H-Y., Yan, W., Tong, L., & Mai, Y-W. "Modelling composite reinforcement by stitching and z-pinning," in Multi-Scale Modelling of Composite Material Systems, Woodhead Publishing, 2005, pp. 319-355.

Topzeven, "Meshes, Plastic mesh, Nylon (PA) mesh (woven)," available at: https://www.topzeven.com/meshes-2/plastic-mesh-nylon-pa-mesh/?lang=en, Accessed April 2024.

Woigk, W., Zhang, B., Jones, M.I., Kuhtz, M., Hornig, A., Gude, M., & Hallett, S.R. "Effect of saw-tooth ply drops on the mechanical performance of tapered composite laminates," Composite Structures, Vol. 272, 2021, p. 114197.

Zhang, J., Lin, G., Vaidya, U., & Wang, H. "Past, present and future prospective of global carbon fibre composite developments and applications," Composites Part B: Engineering, Vol. 250, 2023, p. 110463.